TephraNZ: a major and trace element reference dataset for glass-shard analyses from prominent Quaternary rhyolitic tephras in New Zealand, and implications for correlation

5

Jenni L. Hopkins[1], Janine E. Bidmead[1], David J. Lowe[2], Richard J. Wysoczanski[3], Bradley J. Pillans[4], Luisa Ashworth[1], Andrew B.H. Rees[1], Fiona Tuckett[1]

[1]School of Geography Environment and Earth Science, Victoria University of Wellington, Wellington, PO Box 600, New Zealand
10 [2]School of Science/Te Aka Mātuatua, University of Waikato, Hamilton, Private Bag 3105, New Zealand 3240
[3]National Institute of Water and Atmospheric Research, Wellington, Private Bag 14901, New Zealand
[4]Research School of Earth Science, Australian National University,

Correspondence to: Jenni L. Hopkins (jenni.hopkins@vuw.ac.nz)

Abstract

15   Although analyses of tephra-derived glass shards have been undertaken in New Zealand for nearly four decades (pioneered by Paul Froggatt), our study is the first to systematically develop a formal, comprehensive, open access, reference dataset of glass-shard compositions for New Zealand tephras. These data will provide an important reference tool for future studies to identify and correlate tephra deposits and for associated petrological and magma-related studies within New Zealand and 20 beyond. Here we present the foundation dataset for "TephraNZ", an open access reference dataset for selected tephra deposits in New Zealand.

      Prominent, rhyolitic, tephra deposits from the Quaternary were identified, with sample collection targeting original type sites or reference locations where the tephra's identification is unequivocally known based on independent dating and/or mineralogical techniques. Glass shards were 25 extracted from the tephra deposits and major and trace element geochemical compositions were determined. We discuss in detail the data reduction process used to obtain the results and propose that future studies follow a similar protocol in order to gain comparable data. The dataset contains analyses of glass shards from twenty-three proximal and twenty-seven distal tephra samples characterising 45 eruptive episodes ranging from Kaharoa (636 ± 12 cal. yrs BP) to the Hikuroa Pumice member (2.0 ± 30 0.6 Ma) from six or more caldera sources, most from the central Taupō Volcanic Zone. We report 1385 major element analyses obtained by electron microprobe (EMPA), and 590 trace element analyses obtained by laser ablation (LA)-ICP-MS, on individual glass shards.

      Using PCA, Euclidean similarity coefficients, and geochemical investigation, we show that chemical compositions of glass shards from individual eruptions are commonly distinguished by major 35 elements, especially CaO, TiO_2, K_2O, FeO_t (Na_2O+K_2O and SiO_2/K_2O), but not always. For those tephras with similar glass major-element signatures, some can be distinguished using trace elements (e.g. HFSEs: Zr, Hf, Nb; LILE: Ba, Rb; REE: Eu, Tm, Dy, Y, Tb, Gd, Er, Ho, Yb, Sm), and trace element ratios (e.g. LILE/HFSE: Ba/Th, Ba/Zr, Rb/Zr; HFSE/HREE: Zr/Y, Zr/Yb, Hf/Y; LREE/HREE: La/Yb, Ce/Yb).

40   Geochemistry alone cannot be used to distinguish between glass shards from the following tephra groups: Taupō (Unit Y in the post-Ōruanui eruption sequence of Taupō volcano) and Waimihia (Unit S); Poronui (Unit C) and Karapiti (Unit B); Rotorua and Rerewhakaaitu; and Kawakawa/Ōruanui, and Okaia. Other characteristics, including stratigraphic relationships and age, can be used to separate and distinguish all of these otherwise-similar tephra deposits except Poronui and Karapiti. Bimodality 45 caused by K_2O variability is newly identified in Poihipi and Tahuna tephras. Using glass-shard compositions, tephra sourced from Taupō Volcanic Centre (TVC) and Mangakino Volcanic Centre (MgVC) can be separated using bivariate plots of SiO_2/K_2O vs. Na_2O+K_2O. Glass shards from tephras derived from Kapenga Volcanic Centre, Rotorua Volcanic Centre, and Whakamaru Volcanic Centre have similar major- and trace-element chemical compositions to those from the MgVC, but can overlap

50 with glass analyses from tephras from Taupō and Okataina volcanic centres. Specific trace elements and trace element ratios have lower variability than the heterogeneous major element and bimodal signatures, making them easier to fingerprint geochemically.

1. Introduction

Tephrochronology is the method by which volcanic ash (tephra) deposits are used as
55 stratigraphic isochronous marker horizons (isochrons) for correlating, dating, and synchronising deposits and events in geologic, palaeoenvironmental, and archaeological records (Sarna-Wojcicki, 2000; Shane, 2000, Dugmore et al., 2004; Lowe, 2011; Alloway et al., 2013). In regions where rates of volcanism are high, and eruptive products are widespread, tephrochronology is an essential tool in many aspects of geoscience and associated research (e.g. Hopkins et al., 2021). Geochemical fingerprinting of
60 the glass shards within the tephra deposits is one of the most common ways in which tephra are correlated. Traditionally, major elements were used for correlations (e.g. Westgate and Gorton, 1981; Froggatt, 1983, 1992), but more recent studies have included minor and trace element compositions as well (e.g. Westgate et al., 1994; Pearce et al., 2002, 2004, 2007; Pearce, 2014; Knott et al., 2007; Allen et al., 2008; Denton and Pearce, 2008; Turney et al., 2008; Westgate et al., 2008; Kuehn et al., 2009;
65 Hopkins et al., 2017; Lowe et al., 2017).

Trace elements are more strongly partitioned by fractional crystallisation processes that occur during the formation of melts, and therefore have the potential to be unique for discrete eruption episodes (e.g. Pearce et al., 2004). Specifically, a number of key trace elements have been identified as important for the correlation of rhyolitic tephras, including the high field strength elements (HFSEs) Zr
70 and Nb; the large ion lithophile elements (LILEs) Rb, Sr, and Ba; the heavy rare earth elements (HREEs) Gd, Yb, Sc, and Y; and the light rare earth elements (LREEs) La and Nd. Trace element ratios are also identified as important, including: (1) HFSE/HREE – for example Zr/Y, Nb/Y, Hf/Y; (2) LILE/HFSE – for example Ba/Th; (3) LREE/HFSE – for example Ce/Th, La/Nb; (4) LREE/HREE – for example La/Yb, Ce/Yb; and (5) HFSE/HFSE – for example Zr/Nb, Zr/Th. Some studies have shown
75 that trace elements and trace element ratios can distinguish between tephra beds that have indistinguishable glass-shard major element signatures and thus are a robust way of providing accurate correlations (e.g. Westgate et al., 1994; Pearce et al., 1996; 2002; 2004; Allan et al., 2008; Hopkins et al., 2017).

Tephra correlation is also increasingly being quantified through statistical approaches on
80 geochemical data (Lowe et al., 2017), but many of these approaches (e.g. supervised learning) often require a robust, comprehensive set of "known" reference data against which to test the analyses of "unknown" samples. Statistics can also scale data to make them comparable, but they cannot account or correct for inter-laboratory or historical variance in analyses. Therefore, incomplete datasets, or datasets

constructed from a range of data sources, will limit the ability to provide holistic statistical correlations
85   with accurate outputs. Consequently, the formation of reference datasets that are run in one analytical
session, in one lab, with a consistent methodology are highly desirable for minimising sources of error.
The production of tephra databases is thus being recognised as an exceptionally useful tool
internationally (e.g. Lowe et al., 2017), made more obtainable with open access journals and online,
effectively limitless storage, leading to easier publication and maintenance of large data repositories.
90   Ideally, a global tephra database would exist, but at present this is beyond the scope and remit of any
individual researcher, research group or institute(s). Therefore separate, regional databases for
volcanically active (and other) regions are becoming increasingly popular, such as TephraKam –
Kamchatka (Portnyagin et al., 2020); Tephrabase – Europe (Newton, 1996); AntT tephra database –
Antarctic ice cores (Kurbatov et al., 2014); Alaska Tephra Database (Wallace, 2018); Klondyke
95   Goldfields, Yukon (Preece et al., 2011); VOLCORE – DSDP, ODP, and IODP marine tephra deposits
(Mahony et al., 2020). In addition, in an effort to produce comparable global datasets Abbott et al
(2021) have recently presented guidance for best practices, providing recommendations and templates
for tephra collection, sample preparation, and physical and geochemical analysis.

1.1. Geologic Setting

100   The volcanically active nature of New Zealand (Mortimer and Scott, 2020), and the longevity
and consistency of large-scale rhyolitic eruptions (Howorth, 1975; Froggatt and Lowe, 1990; Houghton
et al., 1995; Wilson et al., 1995a, 2009; Jurado-Chichay and Walker, 2000; Carter et al., 2003; Briggs et
al., 2005; Wilson and Rowland, 2016; Barker et al., 2021) mean the landscape currently has a very long,
detailed, and complex rhyolitic tephrostratigraphic framework that is used for a wide range of
105   applications (Hopkins et al., 2021). However, at present New Zealand tephra studies are lacking a
comprehensive reference dataset resource that has been developed in a systematic way.
          The first large rhyolite-producing eruptions in the Quaternary in New Zealand were sourced
from the Coromandel Volcanic Zone (CVZ) (Carter et al., 2003; Briggs et al., 2005), including from the
Tauranga Volcanic Centre (TgaVC) from c. 3.0 to 1.9 Ma (Pittari et al., 2021). At or after ~2 Ma,
110   volcanism moved into the Taupō Volcanic Zone (TVZ), currently the most active rhyolitic system on
Earth (Wilson et al., 1995a, 2009; Wilson and Rowland, 2016). Nine calderas are recognised within the
TVZ : Mangakino (1.6–1.53 Ma and 1.2–0.9 Ma); Kapenga (0.9–0.7 Ma, 0.3–0.2 Ma, and ~0.06 Ma);
Whakamaru (0.35–0.32 Ma); Reporoa (~0.23 Ma); Rotorua (~0.22 Ma); Ohakuri (~0.22 Ma); Maroa
(0.32–0.013 Ma); Taupō (0.32–0.0018 Ma); and Okataina (~0.6–0 Ma) (**Fig. 1B**; Houghton et al., 1995;
115   Wilson et al., 1995a, 2009; Gravely et al., 2006, 2007; Pittari et al., 2021). The TVZ is further
subdivided into the "old TVZ", which is defined as being active from inception to the Whakamaru
eruptives (~0.34 Ma), and the "young TVZ", which is defined as being active from the Whakamaru
eruptives to the present. "Modern TVZ" is also used to describe the activity since the Rotoiti eruption

(which includes the Rotoiti Ignimbrite, the Rotoehu Ash, and Matahi Scoria members) ~45-47 ka (Danišík et al., 2012; Flude and Storey et al., 2016; Hopkins et al., 2021) to the present (Wilson et al., 1995a, 2009). In addition to these rhyolitic caldera sources in the TVZ and CVZ, the peralkaline rhyolitic Tuhua/Mayor Island (MI) volcano (**Fig. 1**), forming the Tuhua Volcanic Centre (TuVC) (Froggatt and Lowe, 1990), is responsible for erupting the Tuhua tephra (7637 ± 100 cal. yr BP; Lowe et al., 2019) and at least six other MI-derived tephras (Shane et al., 2006). Tuhua tephra is a well-recognised mid-Holocene rhyolitic marker horizon within the New Zealand geologic record due to its distinctive peralkaline geochemistry and mineralogy (Buck et al., 1981; Hogg and McCraw 1983; Froggatt and Lowe 1990; Wilson et al., 1995b; Lowe et al., 1999; Shane et al., 2006; Hopkins et al., 2021).

New Zealand's climatic setting strongly affects tephra dispersal. The landmass sits in the path of predominantly westerly to southern-westerly winds, and therefore the majority of tephra plumes are dispersed to the east of the volcanic zones (Barker et al., 2019). However, tephra deposits from these rhyolitic eruptions are found in a range of different environments, including:

(1) marine (e.g. Nelson et al., 1985; Carter et al., 1995; Alloway et al., 2005; Allan et al., 2008; Lowe, 2014; Hopkins et al., 2020)

(2) lacustrine (e.g. Lowe, 1988; Shane and Hoverd, 2002; Molloy et al., 2009; Shane et al., 2013; Hopkins et al., 2015, 2017; Peti et al., 2020, 2021)

(3) wetlands (e.g. Lowe, 1988; Newnham et al., 1995, 2007, 2019; Lowe et al., 1999, 2013; Gehrels et al., 2006), or

(4) within terrestrially exposed marine or lacustrine sediments, for example in the
- Whanganui Basin (e.g. Seward, 1976, Naish et al., 1996; Pillans et al., 2005; Rees et al., 2019, 2020),
- Wairarapa region (e.g. Shane and Froggatt, 1991; Shane et al.,1995; Nicol et al., 2002), or
- Hawke's Bay region (e.g. Erdman and Kelsey, 1992; Bland et al., 2007; Orpin et al., 2010; Hopkins and Seward, 2019) (**Fig. 1**).

Because of their pervasive nature, high repose period, and high preservation potential, tephra deposits are a common stratigraphic and chronological aid in many studies in New Zealand (Shane 2000; Lowe 2011; Hopkins et al., 2021). For example, the eruption of Kaharoa (636 ± 12 cal. yr BP, Hogg et al., 2003) from Mt Tarawera in the Okataina Volcanic Centre (OVC) has been used to date the arrival of Polynesians in northern New Zealand and map their expansion and impact across the country (Newnham et al., 1998; Lowe and Newnham, 2004). The Rerewhakaaitu eruption (17,496 ± 462 cal. yr BP; Lowe et al., 2013), sourced from OVC, is used as a marker horizon for the transition between the last glacial and present interglacial (Newnham et al., 2003), and several other widespread late Quaternary tephra deposits form boundaries or key stratigraphic markers in the New Zealand Climate Event Stratigraphy developed by the NZ-INTIMATE community (e.g. Kawakawa/Oruanui tephra; Barrell et al., 2013; Lowe et al., 2013). Compositions of glass and mineral components from rhyolitic

tephra deposits have also been used to reconstruct changes in magmatic systems, and give insight into the complexity of caldera-related eruption episodes (e.g. Smith et al., 2002, 2005; Cooper et al., 2012; Barker et al., 2016, 2021; Wilson and Rowland, 2016).

Many of the commonly found rhyolitic tephra horizons in New Zealand are well studied, dated, and geochemically and mineralogically characterised. However, often these studies have been eruption-, source-, or depocentre-specific, and thus only provide a small, effectively piecemeal catalogue of tephra geochemistry that is not necessarily comparable to those of other studies. In addition, compositional data are not usually published in their entirety, or not at all, meaning future studies cannot access nor use the data for correlation techniques. Furthermore, Lowe et al. (1999) identified that differing procedural methods employed at different institutes around New Zealand before and after 1995 produced variable elemental concentrations for the same tephra (post-1995 SiO_2 values were lower by 0.5–1.0 wt.%, and all other elements had slightly higher values). Therefore, it is likely that some of the older tephra compositions that have been relied upon in the past for correlative purposes are no longer appropriate.

It is therefore timely for a comprehensive, systematic, and accessible New Zealand tephra database to be established and curated. In this study we present "TephraNZ" as a foundation reference dataset of internally consistent, open-access data for major and trace element compositions of glass shards from a selection of the most pervasive Quaternary tephra deposits in New Zealand (**Table 1**). This is by far the most complete dataset of New Zealand tephra-derived glass-shard compositions published to date. We discuss in detail the sample preparation, methods of analysis, data reduction and data quality control processes used to generate the results and interrogate the data, thereby providing a template for future studies to produce comparable datasets. Using the glass-shard data obtained, we present an overview of the geochemical variability for a range of rhyolitic tephras of the TVZ; we suggest key geochemical parameters that can be used to identify the individual tephra layers, and apply common statistical techniques to explore the data. Finally, we propose some future avenues of study, utilising these data, which would aid in the progression of a formal, holistic New Zealand tephrostratigraphical framework. Limitations of the dataset are also considered.

2. Methods

2.1. Sample selection, collation, and collection

Key rhyolitic marker horizons were the focus of our foundation dataset. Tephras younger than the Rotoehu Ash (together with Rotoiti Ignimbrite; see **Table 1**) are generally well recognised in the literature and commonly used as tephrochronological marker horizons, therefore these were an obvious choice for the reference dataset. However, for studies using tephra(s) as marker horizons in older deposits 45 ka–2.0 Ma, there are limited well known marker horizons published in the literature. The

most well-studied and accurately dated are those found in the Wanganui Basin (e.g. Pillans et al., 2005 Pillans, 2017). Although not necessarily "key marker horizons" yet, these tephras were chosen to be included in this study for a range of reasons including: (1) they are well dated (mostly) through direct dating techniques; (2) they fall in an important and useful time window; (3) they are stratigraphically constrained and therefore a (mostly) chronologically continuous record; (4) they are thick (although over thickened in some cases) distal deposits and therefore likely represent dominant (pervasive) horizons in the geologic record; (5) some have been correlated with offshore deposits (e.g. Alloway et al., 2005; Allen et al., 2008) or other terrestrial deposits (e.g. Shane and Froggatt, 1991; Shane et al., 1996; Hopkins and Seward 2019) and therefore are useful as geochronological correlatives as we discuss later (**Sect. 4.3.2**); and (6) their locations are very well documented and therefore could be used as tephra type sites or reference sites in future studies.

Known tephra samples in personal collections were collated, prepared, and reanalysed for this study. Where samples were lacking for key tephra deposits, their type localities were found, and samples were obtained through new field work (**Fig. 1**). **Table 1** provides full details of all the sample locations including their status as either proximal (0-10s km from source) or distal (10-100s km from source) and GPS co-ordinates for their exact sampling location. We note here that we have not attempted to sample multiple tephra beds from a single eruptive episode in proximal sequences, nor deposits of the same tephra at different azimuths, as has been undertaken in some more localised or petrologically-focussed studies (e.g. Shane et al., 2005, 2008). We recognise this limitation but instead have concentrated on analysing a wide range of pervasive rhyolitic tephras, both proximal and distal, in a systematic and well-documented way so that future tephrostratigraphic studies will have a foundation of new, high-quality glass-shard compositional data for facilitating robust correlations and applications. Where we have both, we compare proximal and distal analyses of the same tephra and comment on similarities or differences allowing for an increased understanding of the variability in the geochemistry seen in the pyroclastic products of some eruptions. In addition, we have used statistical methods to demonstrate the integrity of our new datasets (and show how such methods can enable unknown tephras to be classified).

2.2. Sample preparation

Bulk tephra samples were disaggregated in water for 1–5 min in an ultra-sonic water bath. Clays and ultra-fines (< 5 µm) were rinsed off and samples were then wet sieved using disposable sieve cloths to 125–250 µm or, where necessary, 60–125 µm. Samples were then dried for 12–24 hr at 50º C before mounting in epoxy resin. Seven samples were mounted into individual drill holes (4-mm diameter) in 25 mm epoxy round blocks (a 4:1 ratio of EpoTek 301 resin [A]: hardener [B]). Individual drill holes were then backfilled using the same epoxy mix (see Lowe, 2011, p. 124, for a schematic illustration). Sample blocks were polished using the following sequence: ~3 min in a figure of eight pattern on 800

225 grit paper with water lubricant to remove the epoxy and break through to the glass shards, ~1 min on 1200 grit paper with water lubricant to remove any large scratches, and ~1 min on 2500 grit paper with water lubricant to begin to reveal the outline of the shards. Blocks were then moved on to the diamond laps with their appropriate lubricant, all at 280 revolutions min^{-1} rotating the block 90 degrees every 30 s followed by 2 min of ultrasonic bathing at < 24 ºC between each lap stage to remove any loose

230 material on the surface of the blocks: ~ 3 min on 6 μm, ~ 1 min at 3 μm, and ~ 1 min at 1 μm. Blocks were then carbon coated before loading in the electron microprobe system for analysis.
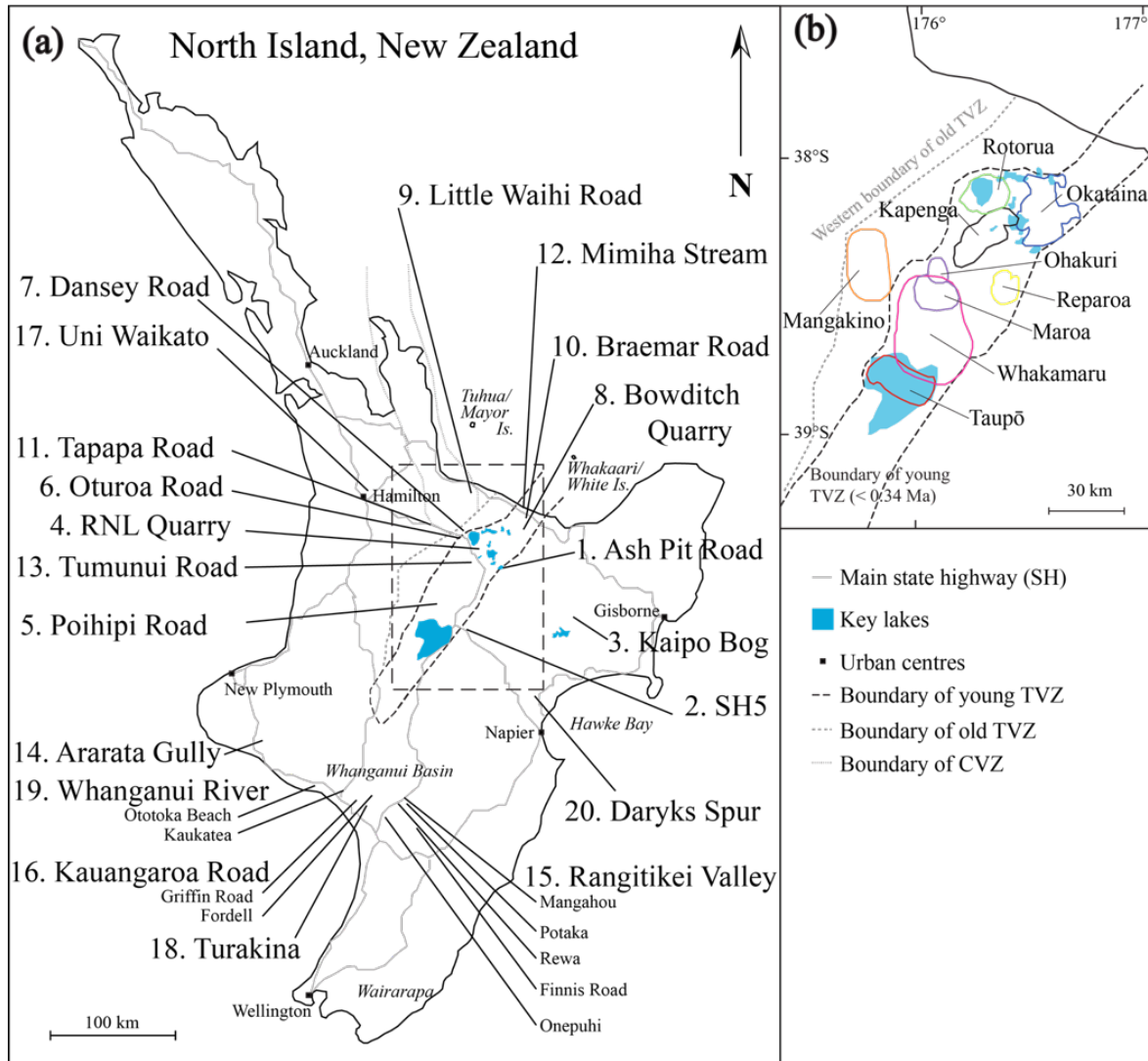
Figure 1. (a) Map of the North Island, New Zealand, detailing the samples sites where the reference tephra deposits for the TephraNZ database were collected. Outlines of CVZ (Coromandel Volcanic Zone) and TVZ (Taupō Volcanic Zone) are shown by dashed lines.

Exact co-ordinates for all sample sites are detailed in Table 1. (b) Inset, outline shown in (a), the calderas of TVZ (details from Houghton et al., 1995; Wilson et al., 1995a , 2009; Gravely et al., 2006, 2007); outline colours of the calderas are used throughout this article in graphs to link the tephra data with their source caldera, if known.

2.3. EPMA method and data reduction

240　　　　Major element analysis of glass shards was undertaken at Victoria University of Wellington (VUW) by wavelength dispersive X-ray spectroscopy (WDS) on a JEOL JXA8230 Superprobe electron probe microanalyser (EPMA). Broadly the method follows that espoused by Kuehn et al. (2011). Backscatter electron images of each sample were taken and used as block maps to allow the location of EPMA analyses to be replicated for trace element analysis. A defocused circle beam 10 µm in diameter

245　was used at 8 nA and 15kV to analyse all major elements as oxides (SiO_2, TiO_2, Al_2O_3, FeO_t, MnO, MgO, CaO, Na_2O, K_2O) and Cl. Run duration for each analysis was ~3 min including online correction. During standardisation, Na_2O was run twice, the second time skipping the peak search to reduce the volatilisation of the element, with the second standardisation value then used. **Supplementary Material (SM) Table 1.1 (a&b)** shows the EPMA set up and run times (after Abbott et al., 2021). During the

250　analysis, VG-568 was run as a calibration standard, and VG-A99 and ATHO-G were run as secondary standards (all standard data can be found in **SM Table 3**), with two of each standard (calibration and secondary) analysed between ten sample analyses to monitor machine drift (no machine drift was identified).

　　　　Initial concentrations were determined using the ZAF correction method, with secondary offline

255　data reduction undertaken to all samples and standards to correct for variability in VG-568. Internal correction values were calculated using the GeoREM reference values of VG-568 from Streck and Wacaster (2006; **Eq. 1**) and applied to all the data (**Eq. 2**). Following this, samples were corrected for deviations from 100 wt.% total; this assumes any variation is due mostly to magmatic water, with a very small amount of minor and trace elements (Froggatt, 1983; Lowe, 2011) that are not analysed by the

260　EPMA (**Eq. 3**). The difference is reported as "H_2O_D" in all data tables to allow back calculation to original data values including totals. Results with $H_2O_D \geq 8$ wt% were removed and are listed at the bottom of the table as "outliers" (**SM Table 2**). Accuracy and analytical precision of the standards were calculated, where accuracy is the offset from the reference value for the secondary standards (**Eq. 4**), and precision is the standard deviation of all measured secondary standards throughout a run, reported

265　at 2 standard deviations (sd) to represent a 95% variability.

Eq. (1)　　　　　　*Internal correction value = average(X_m^p/X_r^p)*

where X_m^p = measured concentration of element X of the calibration standard, and X_r^p = reference

270　concentration for element X of the calibration standard (reference values taken from GeoRem preferred values http://georem.mpch-mainz.gwdg.de/).

Eq. (2)   *corrected data = X_m^i/ internal correction value (Eq.1)*

where X_m^i = measured concentration for element X of any sample or standard.

Eq. (3)   *Secondary hydration corrected data = ((corrected data (Eq.2)/total for that sample) x 100)*

Eq. (4)   *offset from standard (accuracy) = (absolute value (X_r^s – averageX_m^s))*

where X_r^s = reference concentration for element X of the secondary standard (GeoRem preferred value; MPI-DING; Jochum et al., 2006), and averageX_m^s = average concentration measured for element X of all analyses of the secondary standard)

2.4. LA-ICP-MS method and data reduction

In situ trace element analysis was undertaken at VUW using laser-ablation inductively-coupled-plasma mass-spectrometry (LA-ICP-MS) where a RESOlution S155-SE 193 nm ArF excimer laser system was coupled with an Agilent 7900 quadrupole ICP-MS. Data for 43 trace elements were acquired using a static spot method, with a 25 µm spot size, ablation time of 30 s, repetition rate of 5 Hz power (method: 10s background/washout count, cleaning spot of 25 µm for three laser pulses to clean the glass shard surface, 20s background count, 30s acquisition, 10 s washout; see **SM Table 1** for full LA-ICP-MS set up details; after Abbott et al., 2021). Synthetic glass standards NIST-612 and NIST-610 were used to tune the ICP-MS and obtain the P/A factors at a range of spot sizes and laser powers. During the analysis, a full range of standards was analysed to determine which produced the most accurate and precise results as a calibration standard, including NIST-612, NIST-610, BHVO2-G, and ATHO-G. StHS6/80-G was analysed as a secondary standard throughout (results of which are discussed below in **Sect 2.5**, and shown in **Fig. 2** and **SM Table 5**), and all standards (calibration and secondary) were analysed twice every ten samples. All data were reduced offline using Iolite v.3™ software (Paton et al., 2011), using ^{43}Ca as the internal standard value (index channel) and the "*Trace_Elements_IS*" data reduction scheme (DRS). The data were reduced against ATHO-G as the calibration standard. No post-processing data reduction was necessary for the trace elements data but outliers were removed; precision and accuracy were calculated on STHS6/80-G as described above (**Eq. 4**).

2.5. Standardisation method

Multiple calibration standards with different trace element concentrations were analysed to determine which would be most suitable for trace element data reduction. Potential calibration standards included NIST-612, NIST-610, BHVO2-G, and ATHO-G. These were each run twice every ten samples, along with secondary standard STHS6/80-G. **Figure 2** shows the STHS6/80-G results of a range of selected, commonly-used trace elements, including Zn (transition metal), Rb (LILE), Zr (HFSE), La (LREE), Yb (HREE), normalised using each of the calibration standards. Overall, the results show that for the lighter masses (e.g. Zn) there is a large variability in the measured STHS6/80-G values across the different standards, but all except BHVO2-G sit within error (2 sd) of the reference value (**Fig. 2)**. For the heavier masses (e.g. La, Yb, **Fig. 2**), the variation from the reference value observed within the analysed values decreases, except for NIST-610, which remains highly variable in the middle masses (Rb, Zr, **Fig. 2**), with variability reducing in the heavier masses. The data show that the use of ATHO-G as the calibration standard (for data reduction of rhyolites) produces the most accurate and precise data for the secondary standard, for all except the elements with the heaviest masses and smallest concentrations (e.g. Yb).

2.6. Statistical methods

2.6.1. Principal component analysis

To visualise elements that distinguish the different tephra compositions we have used principal component analysis (PCA). PCA was run in the coding platform R (R core team, 2019) v3.6.2 and RStudio v.1.2.5033 using packages "ggbiplot" (Vu, 2011), "Hotelling" (Curran, 2018), "ggplot2" (Wickman, 2016), "factoextra" (Kassambara and Mundt, 2020) and "vegan" (Oksanen et al., 2019). Data for Tuhua tephra were removed as these would unnecessarily skew the results due to their distinct geochemistry. Non-normalised, average, elemental values were used from each tephra sample, for example Si in ppm, no oxide values, no ratios (e.g. SiO_2/K_2O) or sums (e.g. Na_2O+K_2O). All element values were centred using a centred log-ratio transform to deal with closure effect (clr: column mean subtracted from each value) and scaled (value divided by the standard deviation of the column) to compare elements with concentrations that differ by orders of magnitude. PCA was run using the "prcomp" (Venables and Ripley, 2002) function, and PCA contributions were calculated using "fviz_contrib" (Kassambara and Mundt, 2020) function. A template of the coding script used can be found in **Supplementary Material 1**.
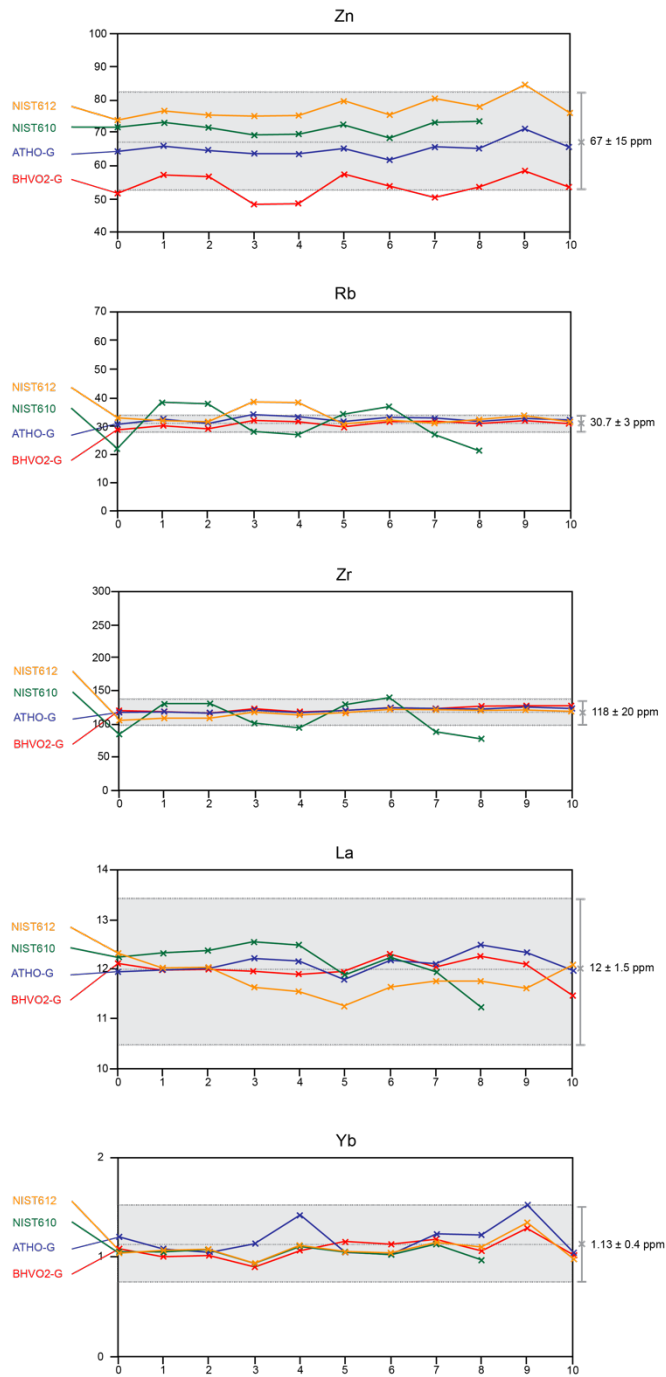
Figure 2. Compilation of trace element standard data produced during the first run of glass-shard analyses. These data show selected element concentrations of secondary standard STHs6/80 normalised using difference calibration standards (NIST-612 – orange; NIST-610 – green, ATHO-G – blue, and BHVO2-G – red). The grey shaded area shows the preferred GeoREM reference value (http://georem.mpch-mainz.gwdg.de/) error margin reported for each element for STHS6/80. Note that for standard NIST610, two data points were removed as outliers; full data can be found in SM Table 5.

340

12

2.6.2. Euclidean similarity coefficients

345   To identify the tephra samples that were most similar, and could therefore pose problems in attempting to obtain unique fingerprinting, we ran Euclidean similarity coefficients (ESC) analysis. ESC was run in R and RStudio using the package "stats" (R core team, 2019). Following the guidelines of Hunt et al. (1995) for ESC analysis, we used non-normalised, mean concentrations of the elements highlighted by the PCA to be the most indicative of variance in the dataset. These values were input as

350   comparison values, and the function "as.matrix.dist" was used to run the "euclidean" distance measure. This method calculates the similarity of samples based on an infinite number of comparison input values. A template of the coding script used can be found in **Supplementary Material 2**. The output table was manipulated post-production to provide the colour formatting shown in **Figure 14**.

3. Results

355   The averages and their standard deviations for all samples are reported in **Table 2**; the full reference dataset can be found in **SM Table 2**. All reported values in the text and figures (unless stated otherwise) are recalculated (normalised) to 100% on a volatile-free basis (following Lowe et al., 2017) with the difference between the raw total and 100% being reported as "H_2O_D" (**Table 2)**. For best correlation results, we recommend that the full dataset is used in order to see the trends in the

360   geochemical data rather than just the means and standard deviations.

3.1. Data quality

    Standard values for VG-568 and VG-A99 are taken from the GeoREM. The reference values used as a standard (by other publications) are from Jarosewich et al. (1980). However, for the purpose

365   of this research we have chosen alternate values published by Streck and Wacaster (2006). A comparison of the reference values from both publications is shown in **SM Table 6** and **SM Figure 6.1**. Most of the values reported are within error of one another for both VG-568 and VG-A99. However, the data set from Streck and Wacaster (2006) is more complete including values for MgO and Cl, which are not reported by Jarosewich et al. (1980). We do note, however, that Cl is challenging to analyse

370   accurately on EPMA for glass due to its low concentration and especially as there are few standards that have similar compositions (e.g. Jochum et al., 2006). Our samples have between 0.3 and 0.06 wt% Cl, therefore VG-568 (with Cl = 0.1 wt%), ATHOG (with 0.04 wt%), and VG-A99 (with 0.02 wt%) attempt to provide a good range for standard comparison.

    Figures plotted in **SM Table 3 (SM Fig. 3.2, 3.3, and 3.4)** show the variability in the

375   concentrations analysed by the EPMA of the standard data throughout the running of these samples. For the secondary standards ATHO-G (**SM Fig. 3.3**) and VG-A99 (**SM Fig. SM 3.4**), there is some clear

variability within the batches of samples run. For example for SiO_2 for ATHO at point 60, there is a clear jump in the values reported, for Na_2O for ATHO at points 92–101 there are some very low concentrations, and for MgO for VG-A99 there are clear variations in different run sets. The variation observed in all these data is likely due to a number of factors including: (1) a change to a different standard shard during the run; (2) re-calibration of the EPMA after a period of down time (note the dates of analyses) and/or (3) day-to-day variations in machine performance; (4) for the case of Na_2O, possible volatilisation of Na_2O due to repeated analysis of the same standard shard; (5) use of an inappropriate primary calibration standard (for example a rhyolite standard (VG568) to calibrate a basaltic glass (VG-A99) which is used in this case as a secondary standard).

Difficulties in accurate analysis of Na_2O, and a suggestion that the reported reference value for ATHO-G from Jochum et al (2006; reported as 3.75 wt.%, but with a range from different analytical techniques of 4.31 – 3.53 wt.%) are too low, has been identified in a number of studies recently (e.g. Lowe et al., 2017; Portnyagin et al., 2020). Our use of Steck and Wacaster (2006) reference data for VG-568 as an internal calibration (3.52 wt.%) rather than the Jarosewich et al (1980) value (3.75 wt.%) brings our secondary standard data in alignment with the original Jochum et al (2006) values for ATHO-G (see **SM Table 3.3**). We also note that other studies (e.g. Rowe et al., 2008; However, it is possible that because of this, our sample values reported for Na_2O are too low. Further studies into this community-wide issue will hopefully allow this discrepancy to be resolved.

During LA-ICP-MS tuning oxide production was monitored using the ThO/Th ratio, and this value was tuned to between 1.3 and 1.8 %, which is considered high by current standards (e.g. Portnyagin et al., 2020 reported values of 0.5–0.7 %), but are comparable with values in older studies (e.g. Jochum et al., 2006 report values "<1-2%"; Pearce et al., 2011 reported values "typically ~ 1.5 %"; Allan et al., 2008 reported values "typically <1%, always <2%"). This high oxide production value could have had impacts on some elements. For example, it is likely that there was a high addition of SiO into our analyses; SiO can interfere with [45]Sc, or alternatively, BaO can interfere with [153]Eu, however, because the concentration of SiO_2 in our samples is similar to that of our secondary standard (ATHO-G), the data should still be viable. In addition, to monitor the impact of oxides on our elements we analyse and report multiple isotopes of Sr (86 and 88), Zr (90 and 91), Mo (95 and 98), Ba (137 and 138), and Eu (151 and 153). The concentrations of these elements do not show significant variability (e.g. **SM Fig. 6.2.3, and 6.2.4**; $R^2_{Sr} = 0.96$, $R^2_{Zr} = 0.99$). In addition, when plotted together, Ba vs. [153]Eu show no relationship (**SM Fig. 6.2.5**), proving little-to-no oxide interference has impacted the values obtained for these elements.

Ti, Mn, Ca and Si were analysed by both EPMA and LA-ICP-MS: **SM Fig. 6.2.1** (Ti) and **SM Fig. 6.2.2** (Mn) show comparative analyses of concentrations measured on the same spots for EPMA vs LA-ICP-MS. For Ti, $R^2=0.63$ suggesting a good agreement between the two methods of analysis. Any anomalous values are indicative of mineral contamination in the LA-ICP-MS analysis (potentially

orthopyroxene or titanomagnetite). For Mn, the $R^2 = 0.26$, showing a poor agreement between the two analysis types. However, this result is likely due to the imprecision afforded by the EPMA analysis on such small concentrations. For future analyses, to allow a full comparison of the elements between the two methods and therefore identification of contamination in the LA-ICP-MS analyses, Portnyagin et al (2020) suggest analysis of all major elements by LA-ICP-MS.

3.2. Major element results

All glass shards analysed are characterised as rhyolitic according to the classification of Le Maitre (1984) (**Fig. 3**), with SiO_2 concentrations (normalised) ranging from 72.5 wt.% to 79.8 wt.% (with the majority 74-79 wt%), and Na_2O+K_2O ranging from 5.8 wt.% to 9.8 wt.%. Three compositional regions with high concentrations of samples are evident within **Figure 3**. These show a negative trend between SiO_2 and Na_2O+K_2O, with each region separated by differing SiO_2 values – for example, $SiO_2 = 76-77$ wt.%, 77.5-78 wt.%, and 78-79 wt.%. Glass samples from the peralkaline Tuhua tephra (TuVC) are identifiable because of their unique (peralkaline) geochemistry, with much higher Na_2O+K_2O (≥ 9 wt.%) for equivalent SiO_2 ($= 73.5-75$ wt.%; Lowe, 1988) in comparison to those of the rhyolitic TVZ-sourced deposits ($Na_2O+K_2O \leq 8.5$ wt.%). Tuhua-tephra-derived glasses also have higher FeO (≥ 5.6 wt.%) and Na_2O (≥ 4.7 wt.%), but lower CaO (≤ 0.8), and Al_2O_3 (≤ 10.1) in comparison to the analyses for the rest of the samples (FeO $= 0.2-2.8$ wt.%, $Na_2O = 2.6-5.1$ wt.%, CaO $= 0.5-2.6$ wt.%, and $Al_2O_3 = 11.8-15.2$ wt.%; **Fig. 4**). For all other major elements, the compositional variation of the Tuhua tephra samples sits within the overall range for the other samples, with $TiO_2 = 0.02-0.55$ wt.%, MnO $= 0.01-0.2$ wt.%, MgO $= 0.01- 0.63$ wt.%, $K_2O = 1.8-6.0$ wt.%, and Cl $= 0.01-0.72$ wt.% (**Fig. 4**).

Of the 45 tephra samples, 22 have a 'homogeneous signature', homogeneity being defined here (as an approximation) when the standard deviation of the sample is equal to or less than analytical error (2sd of secondary standard: for example, for FeO $= \pm 0.23$ wt.%, CaO $= \pm 0.10$ wt.%). The majority (~64%) of the samples that have a homogeneous signature are from OVC (e.g. Whakatane, Mamaku, Rotoma) or from calderas older than OVC (~32%), such as (1) Upper Griffins Road tephra, a correlative of the Whakamaru eruptives, Whakamaru Volcanic Centre (WVC), and (2) Mangapipi tephra, a correlative to deposits of Mangakino Volcanic Centre (MgVC; **Fig. 5a**). Ten samples show a heterogeneous signature (where standard deviations for both FeO and CaO are greater than analytical errors), with most from a proximal source (~30%), or from tephras deposited in the Whanganui Basin area (40%), and with the remainder being from the Mangaone Subgroup eruptives from the OVC: Hauparu, Maketu, and Ngamotu (**Fig. 5b**).

Glass shards from four tephra samples show a bimodal signature in some major and trace elements, where specific elements split the populations into two distinct groups. Tephras showing this phenomenon include Rotorua (OVC), Rerewhakaaitu (OVC), Poihipi (TVC), and Tahuna (TVC). The bimodal signatures of Rerewhakaaitu and Rotorua are well documented (Shane et al., 2008), whereas

those of Poihipi and Tahuna are newly identified here (**Fig. 6**). All four of these tephra horizons have their glass-shard bimodal signatures produced predominantly by K_2O concentrations, into high (≥ 3.8 wt.%) and low (≤ 3.6 wt.%) populations (**Fig. 6**) linked to the crystallisation of biotite minerals. This relationship has been discussed by previous research (for Rerewhakaaitu and Rotorua), and modelled as two different biotite populations formed through fractional crystallisation in a zoned magma chamber (e.g. Shane et al., 2003; Nairn et al., 2004), resulting in the formation of heterogeneity in the magma and hence the formation of different glass compositions.

For five of the tephras, we undertook analyses on glass from both proximal and distal samples. These tephras included Whakatane, Rotoma, Waiohau, Rotorua, and Rerewhakaaitu, which are all derived from OVC (**Table 1**). For Rotoma, Rerewhakaaitu, and Waiohau, the signatures of the proximal and distal deposits are indistinguishable, whereas for Whakatane and Rotorua the proximal signature is highly variable, and the distal signature is homogeneous but overlapping with part of the extent of the proximal signature (e.g. **Fig. 7**). Similar findings are reported and discussed in more detail for Whakatane tephra in Kobayshi et al. (2005) and Holt et al. (2011); and for Rotorua tephra in Shane et al. (2003a) and Kilgour and Smith (2008).

3.3. Trace element results

Figure 8 shows a primitive mantle-normalised spider plot of all the trace element data for the glass shards analysed (after Sun and McDonough 1995). The majority of the data plots along a common pattern of variable concentrations of HFSE, LILEs and LREEs, but they show more consistent concentrations of HREEs (Gd to Lu). Of note are peaks in Nd, a negative Sr anomaly relative to LREE, and a positive Zr-Hf anomaly relative to Sm. Sr and Ba show the largest variability in concentrations that is likely caused by a variability in feldspar crystallisation (Pearce et al., 2004). Several different patterns are observable within this full data suite pertaining to individual samples. The obviously different signature is that for glass from Tuhua tephra which shows a low concentration of Ba (< 10 ppm) and Sr (<1 ppm) in comparison with values for the rest of the samples, and with high concentrations of all other elements, especially the REEs (**Fig. 8**). Analyses of glass shards from the Maketu tephra can also be identified by their high concentrations of all elements in comparison to the TVZ trends but mid-range Nb values (between those of Tuhua and the general trend) (**Fig. 8**). We also note Er and Lu peaks, which pertain to glasses from the Te Rere tephra, that sit at the higher concentration levels of the general trend (these could potentially be analytical artefacts; **Fig. 8; Table 2**), and samples from Ngamotu, Rotoehu/Rotoiti, and Earthquake Flat deposits that sit at the lower overall trace element concentration levels of the general trend (**Fig. 8**). For the tephras where both proximal and distal samples of glass have been analysed for trace elements, the HFSEs (including Zr,

16

Hf, Th, and Ti) and LILEs (including Rb, Sr, and Cs) may exhibit heterogeneity between the proximal and distal samples, whereas the HREE and the LREE tend to have a lower variability (**Fig. 7**).
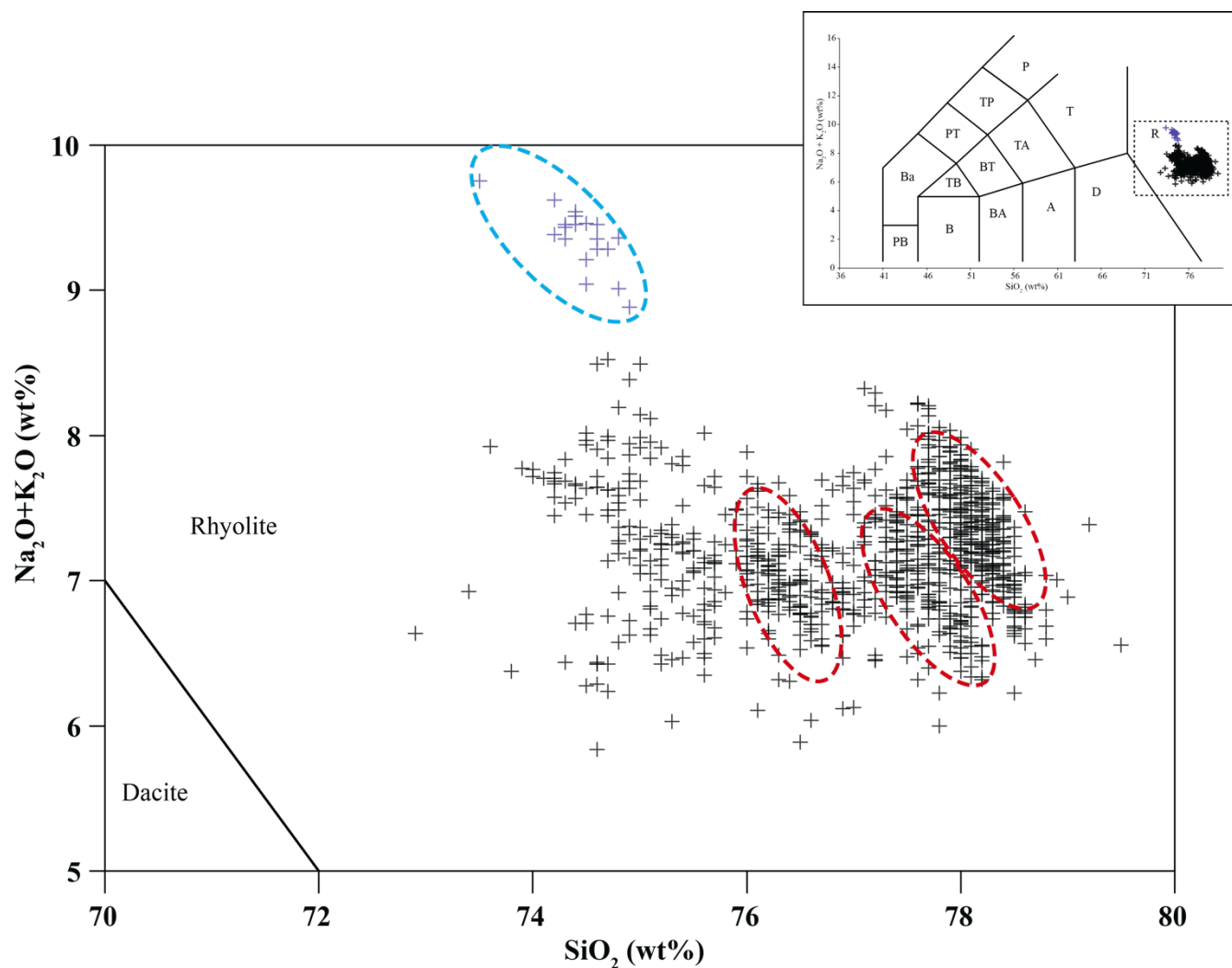

Figure 3. Total alkali (Na$_2$O+K$_2$O) vs. SiO$_2$ (TAS) plot for glass compositions for all reference data (presented on a normalised basis). Identified and highlighted by blue dashed outline are the glass shard compositions for the Tuhua tephra (Mayor Island; MI), and highlighted by the red dashed outlines are the regions on the TAS diagram that show the highest density of samples. The inset shows a full TAS diagram (always on an anhydrous basis) to provide context for the enlarged figure. Regions of the TAS diagram follow the nomenclature of Le Maitre (1984): A – andesite, B – basalt, Ba – basanite, BA – basaltic andesite, BT – basaltic-trachyte, D – dacite, P – phonolite, PB – picro-basalt, PT – phonotephrite, R – rhyolite, T – trachyte, TA – trachy-andesite, TB – trachy-basalt, TP- tephriphonolite.

485

490
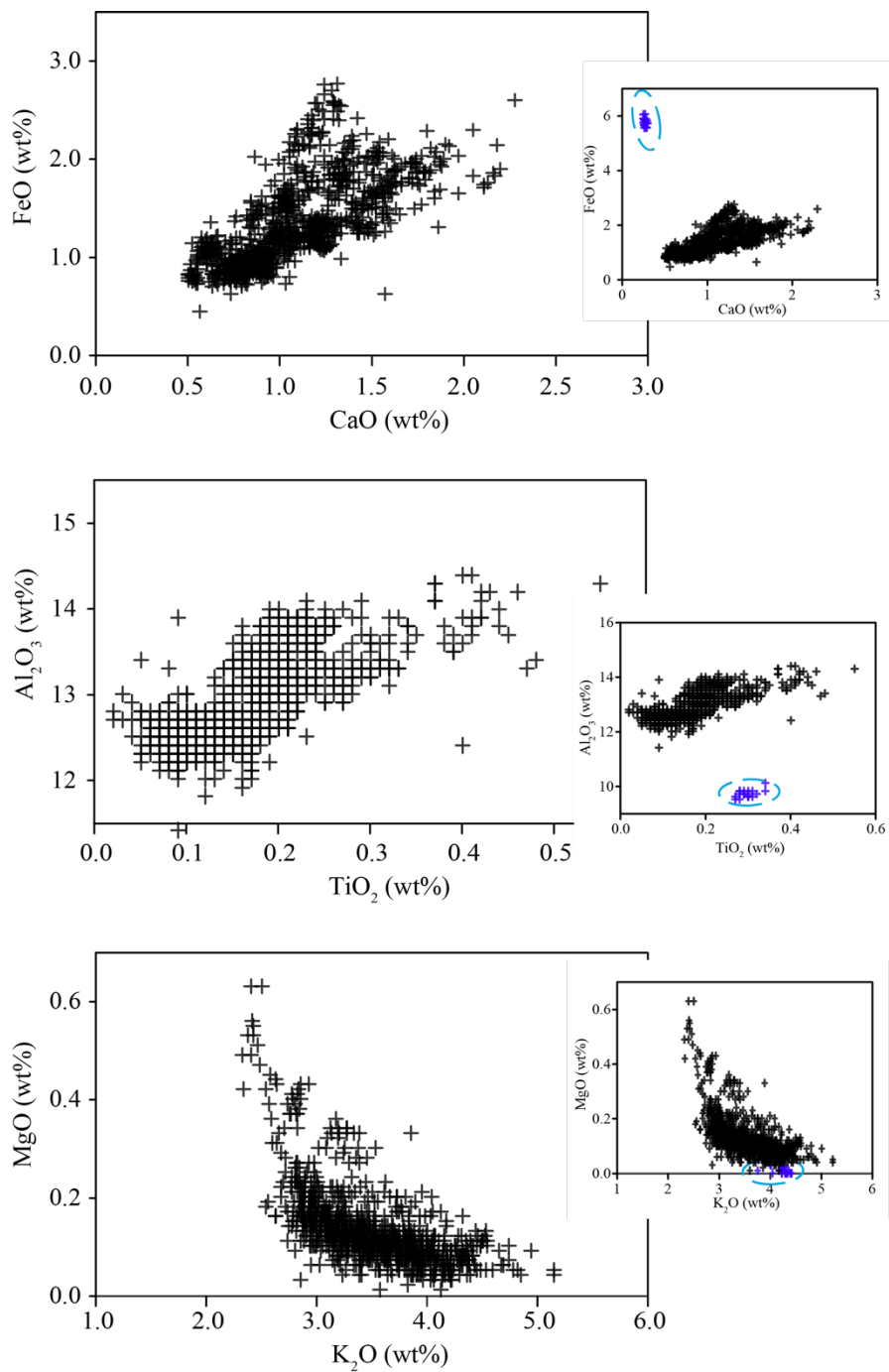
Figure 4. Major element bivariate plots of glass shard compositions for all reference data (presented on a normalised basis). Highlighted in the insets by blue dashed lines are the Tuhua tephra samples. These are removed from the enlarged figure to allow the detail of the majority of the samples to be seen more clearly. Total iron expressed as FeO.
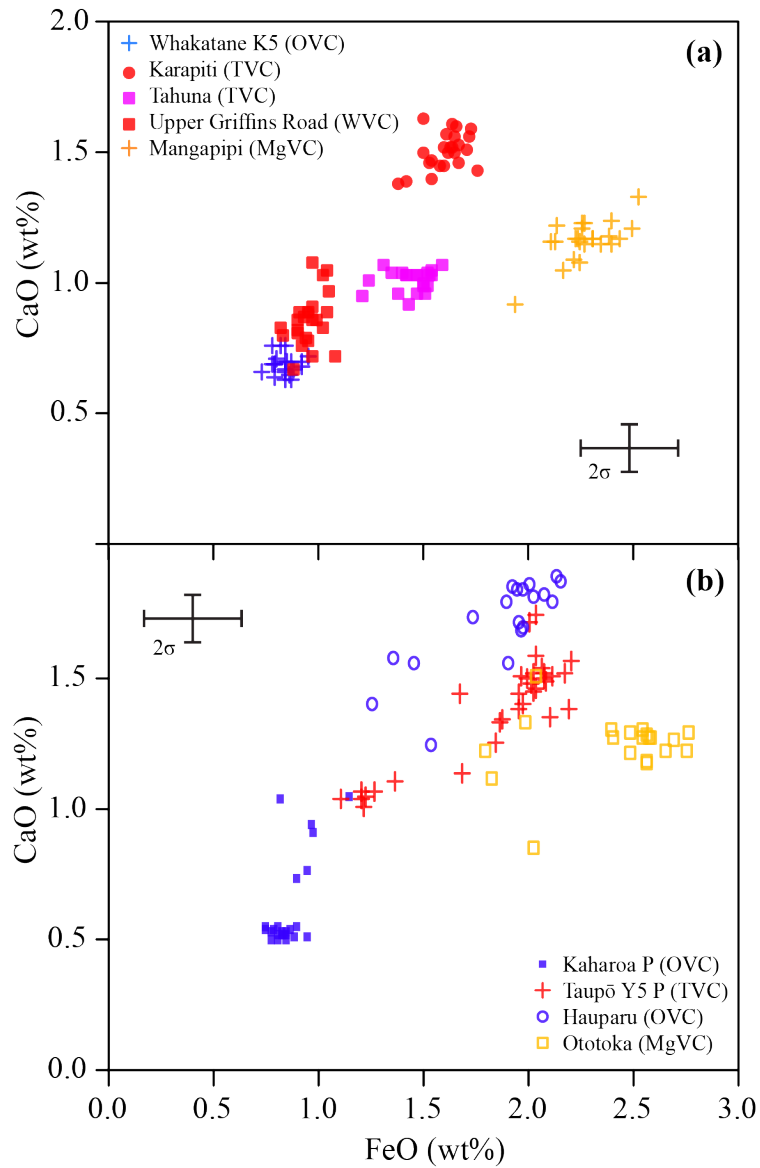
Figure 5. Examples of major element bivariate plots for glass shard analyses of tephras (presented on a normalised basis) which show (a) a homogeneous signatures, where the standard deviation of the analysis is less than the analytical error (shown as 2σ); and (b) heterogeneous signatures, where the standard deviation of the analysis is greater than the analytical error. Different colours indicate the differing caldera sources (shown on Fig. 1) and different symbols show the different tephras. P = proximal sample (see Table 1). Total iron expressed as FeO.
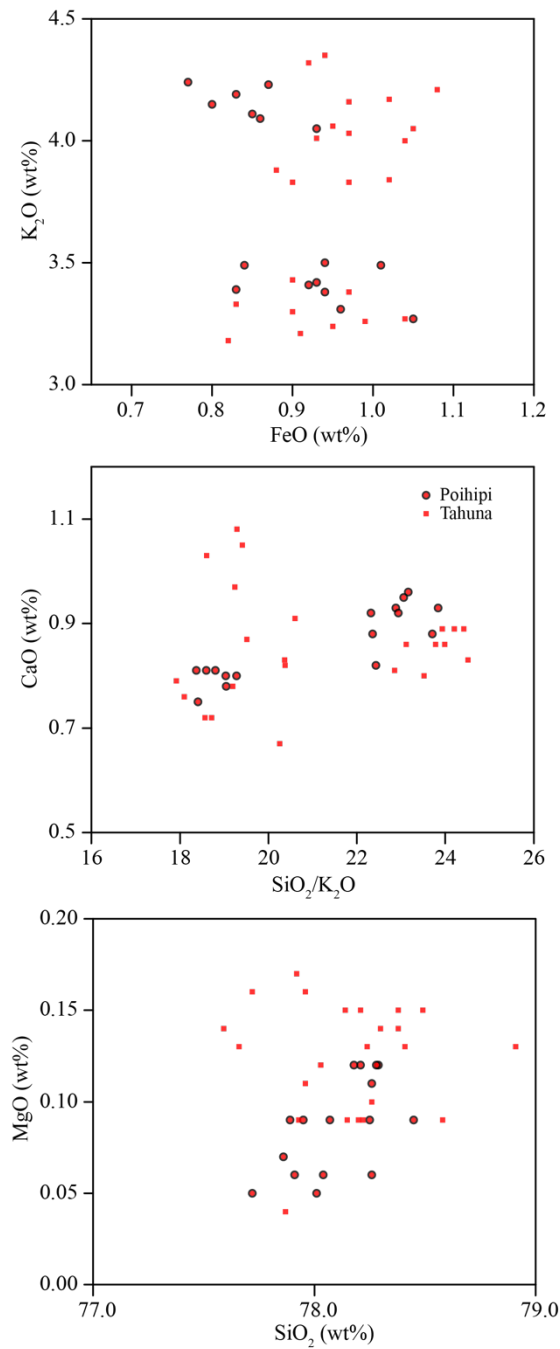
Figure 6. Selected major element biplots of glass analyses (presented on a normalised basis) of samples from Poihipi and Tahuna tephras (both TVC sourced) that exhibit a bimodal signature. This bimodality is identified as being caused by K_2O concentration (e.g. see Lowe et al., 2008; Shane et al., 2008), and therefore plots with other elements (major or trace) do not show this bimodality. Total iron expressed as FeO.
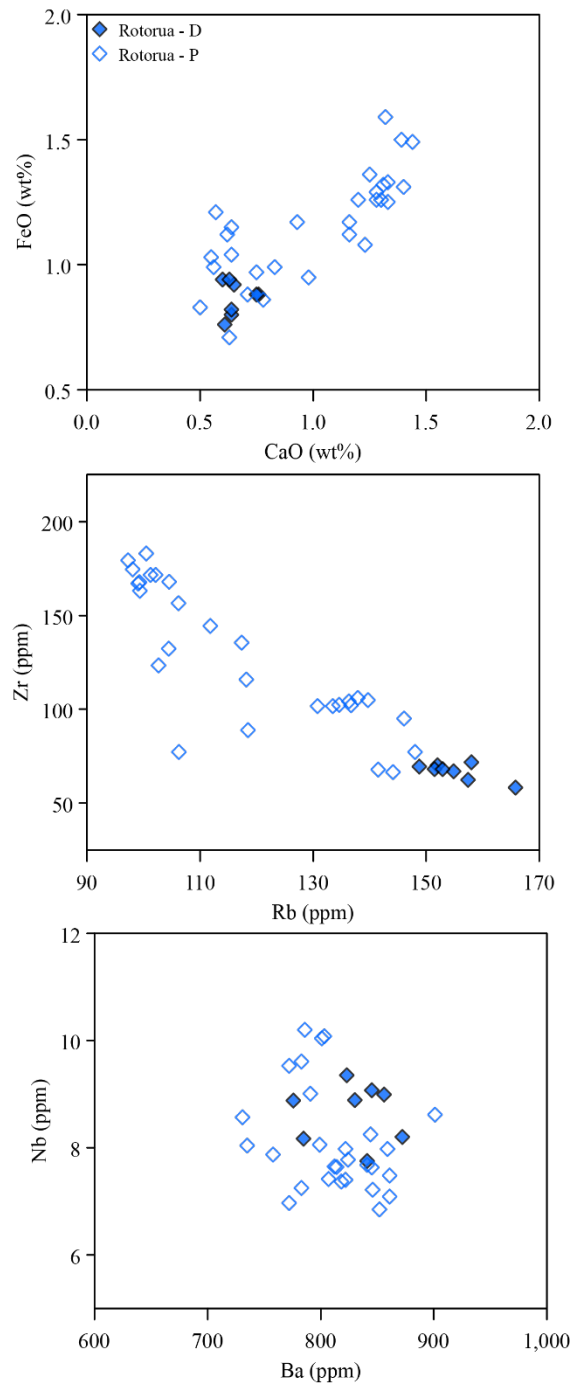
Fig. 7. Major and trace element biplots showing the glass-shard-derived geochemical relationship of Rotorua (OVC) proximal (P) and distal (D) tephra deposits (presented on a normalised basis, total iron expressed as FeO). Distal deposits may have a signature with lower geochemical variability which overlaps within the spread of the heterogeneous proximal signatures. This variation can often be resolved by using trace element plots of selected elements – see text for discussion.
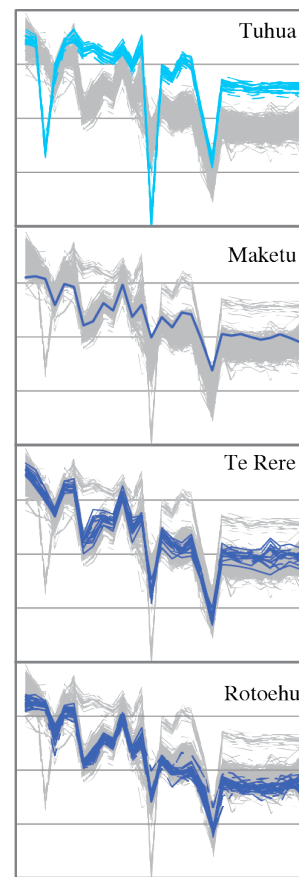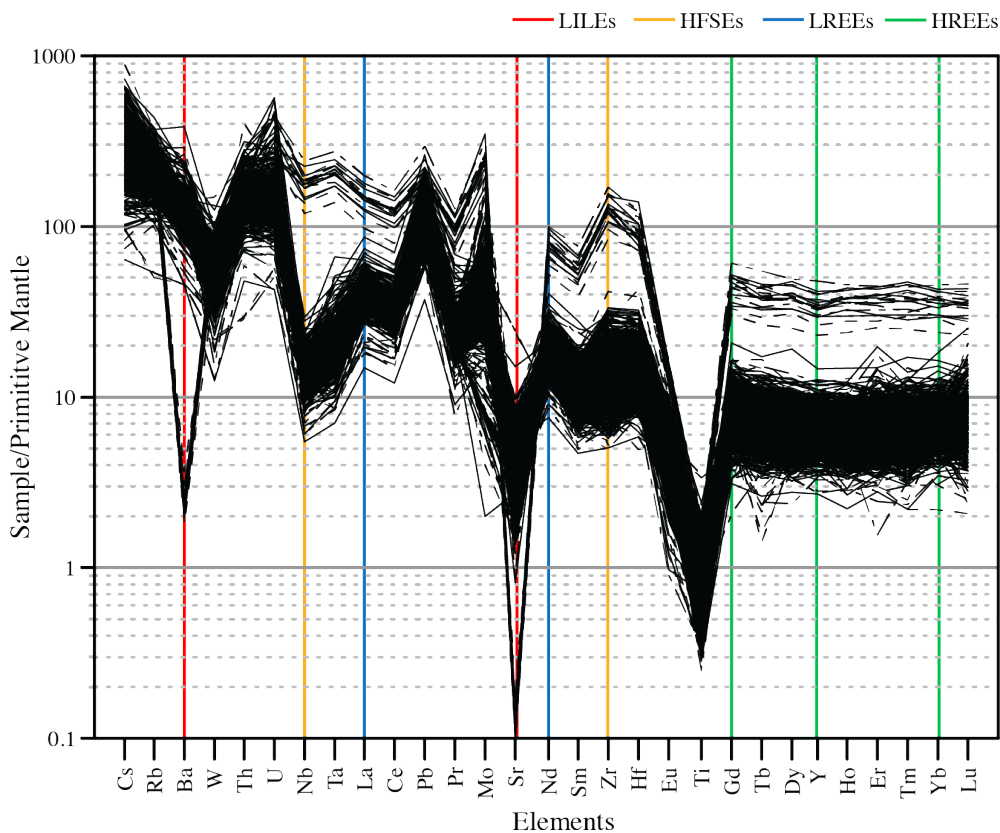
Figure 8. Primitive mantle normalised (McDonough and Sun 1995) trace element spider plot for glass analyses for all reference samples. Highlighted are key elements discussed in the text coloured by their characteristics including HFSE, LILE, LREE, and HREE. The full plot is presented to show the density of data with the dominant trend line plus the obvious deviations from this. The samples which correspond to these deviations are shown in the smaller plots at right, including analyses on glass from Tuhua (MI), Maketu, Te Rere, and Rotoehu (OVC) tephras. The Rotoehu Ash signature is also similar to that for the Rotoiti Ignimbrite (which are coeval deposits; Nairn, 1972), the Earthquake Flat tephra (Kapenga VC; Nairn and Kohn, 1973), and the Ngamotu tephra (OVC; Jurado-Chichay and Walker, 2000).

4. Discussion

4.1. Distinguishing geochemical characteristics

530 #### 4.1.1. Major and trace elements in general

In many cases, the major element concentrations in glass are sufficient to allow different tephras to be distinguished (including through the common use of biplots), a result consistent with the findings from much previous work both in New Zealand and elsewhere (e.g. Lowe et al., 2017). However, previous studies have also shown that for some New Zealand tephras more elements from the glass
535 analyses are often required to distinguish between tephras from different eruptions. For this reason we used principal component analysis (PCA) on the dataset to compare multidimensional data rather than an array of traditional biplots. Looking at data in a multidimensional space can allow variations to be more readily distinguished and visualised because all constituent elements are used, not just two.

PCA results for the glass-shard major elements (**Fig. 9**) show that PC1 and PC2 explain 82.7%
540 of the variance within the data. Al, K, Si, Na, and Ti make the highest contributions to PC1 (**Fig. 9**), while Fe, Mn, and Cl have the greatest loadings on PC2 (**Fig. 9**); therefore, these elements are most appropriate for distinguishing between tephra deposits for the reference dataset as a whole (**Fig. 9**). These major elements, especially Fe and K (± Ca), have long been recognised as being useful to distinguish many New Zealand late Quaternary tephras from one another (e.g. Lowe, 1988; Shane,
545 2000; Alloway et al., 2013); however, the inclusion of Ti, Al, Mn, and Cl are somewhat unusual. In a number of cases (discussed below), however, major element concentrations are shown to overlap for certain tephra horizons, and thus trace elements and trace element ratios are investigated to provide additional variables to use as discriminants. PCA was also applied to scaled trace elements and major elements together, with the results indicating that PC1 and PC2 could explain 62.8 % of the variability
550 in the full data suite with V, Co, Mg, Cu, Ti, Sr, Sc, Ca, Cs, and Zr being the ten highest contributors to PC1, and Cu, Mn, Mg, Cs, Sc, Co, Ti, Sr, Th, and Rb highlighted as the ten highest to PC2 (**Fig. 10**). Therefore, these elements, and the ratios of these elements, have the highest potential to distinguish individual tephra horizons when using their glass-shard compositions alone.
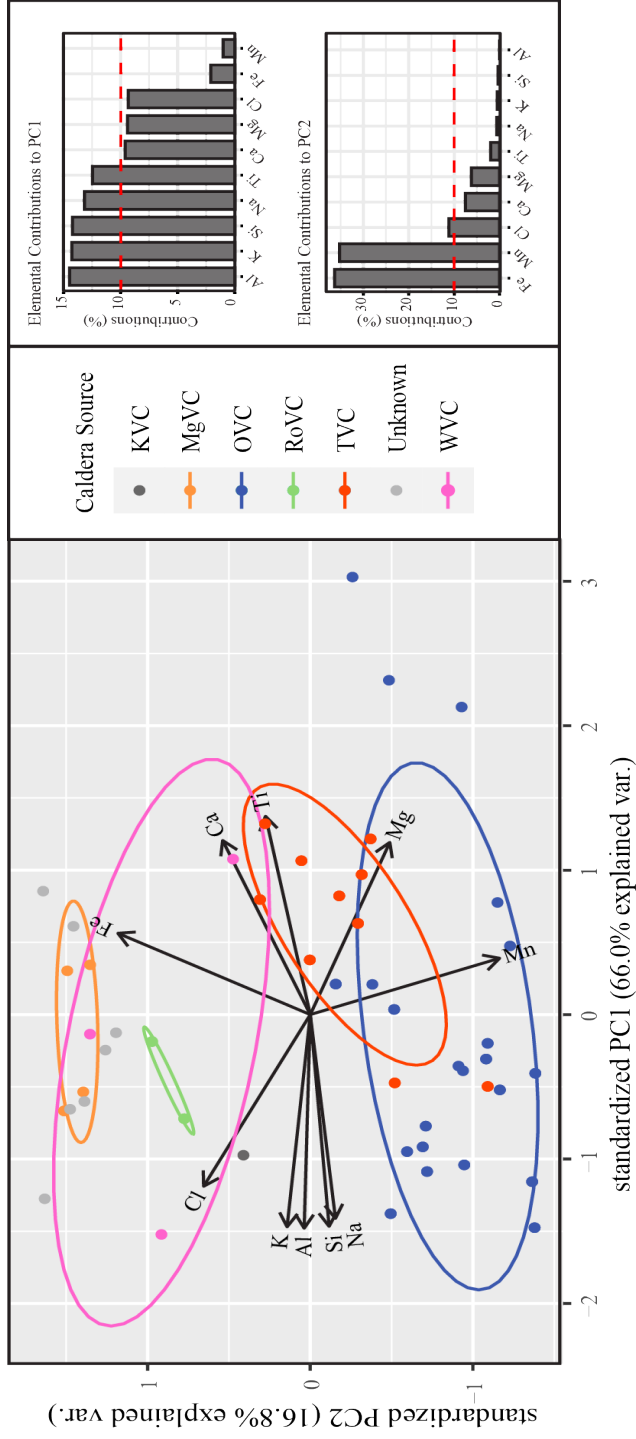
Figure 9. Results of PCA analysis on all TephraNZ major element reference data for glass (normalised). Data are scaled to allow comparison within the PCA analysis. Tephra samples are coloured as per their source centre, and ellipses highlight the mean compositional region for each source caldera (KVC – Kapenga Volcainc Centre, MgVC – Mangakino Volcanic Centre, OVC – Okataina Volcanic Centre, RoVC – Rotorua Volcanic Centre, TVC – Taupō Volcanic Centre, and WVC – Whakamaru Volcanic Centre. PCA analysis was performed in R (see SM1 for R script). Bar plots highlight the top elemental contributions for PC1 and PC2. The red dashed line on the elemental contribution plots indicate the expected average contribution; if the contribution by each element was uniform, the expected value would be 1/no. of variables (e.g. 1/9 = ~11%). Therefore, a variable with a contribution larger than this cut-off line (~11%) is considered important in the contributing to the component.
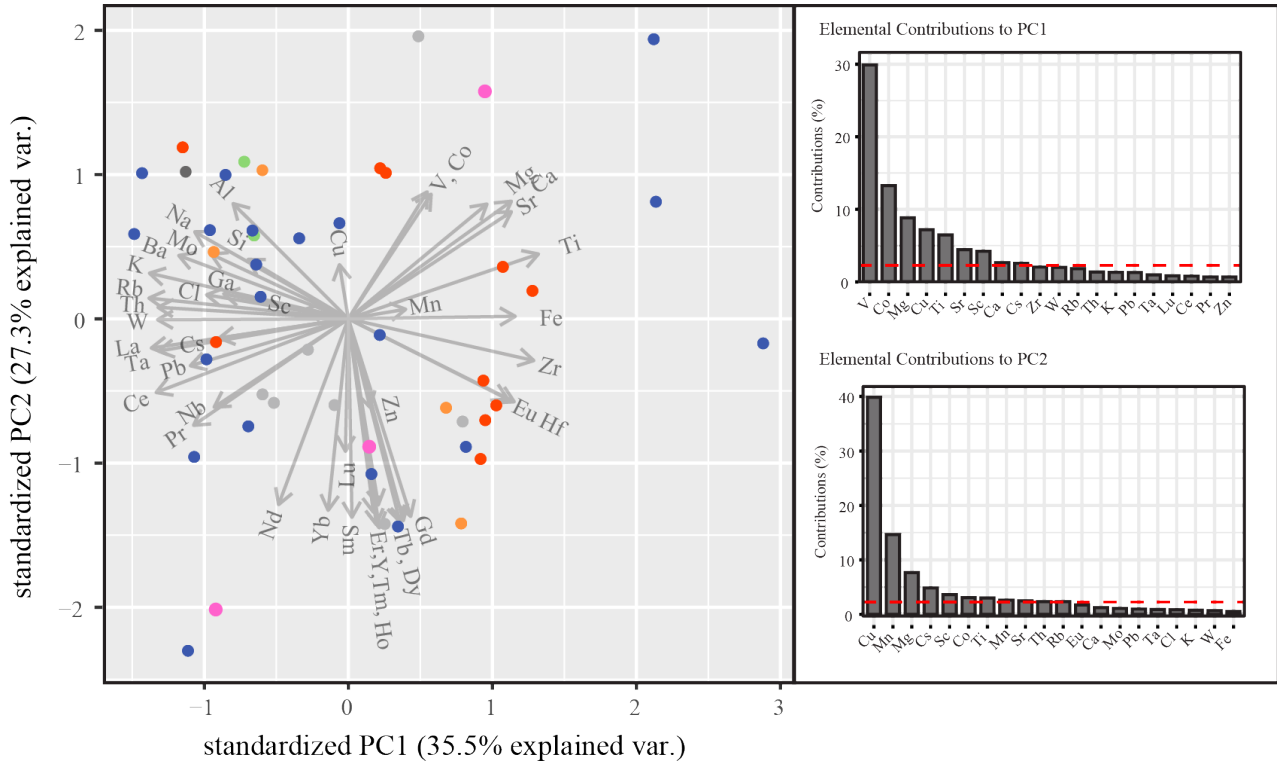
Figure 10. Results of PCA on all TephraNZ reference data for glass. Data are scaled to allow comparison within the PCA analysis. Tephra samples are coloured as per their source centre see key in Figure 9. Mean ellipses have been removed for clarity for this figure. PCA analysis was performed in R (see SM1 for R script). Bar plots highlight the top elemental contributions for PC1 and PC2. The red dashed line on the elemental contribution plots indicates the expected average contribution; a variable with a contribution larger than this cut-off line is considered important in the contributing to the component.
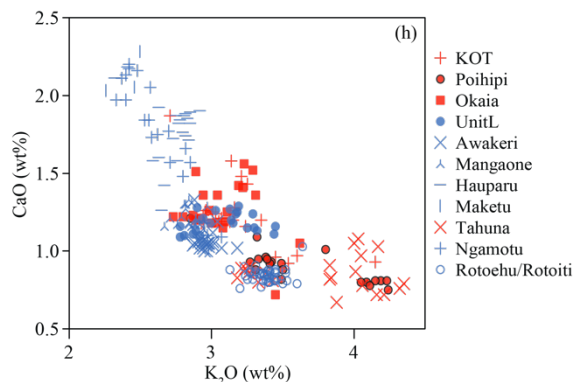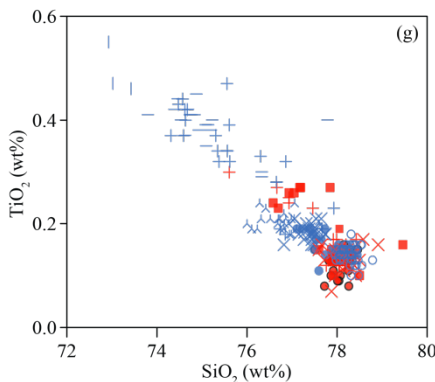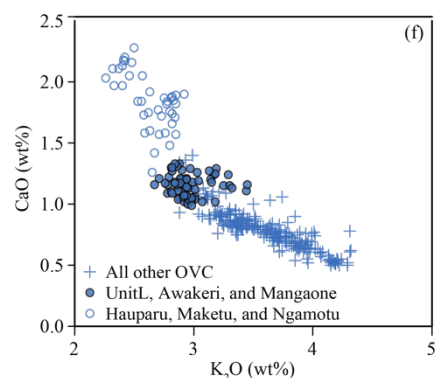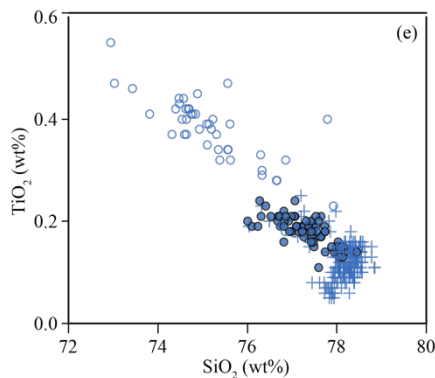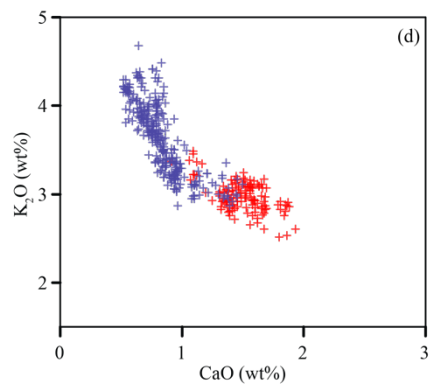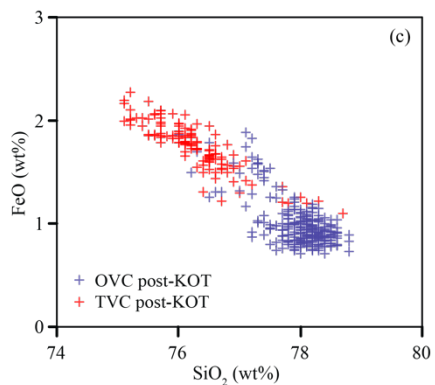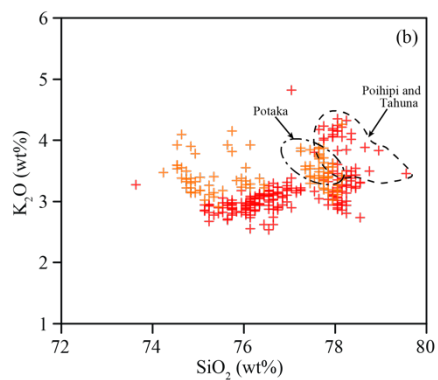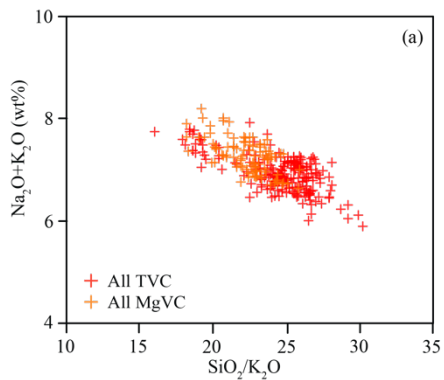
Figure 11. Major element biplots to distinguish between caldera sources of tephras based on their glass major element compositions (presented on a normalised basis; total iron is expressed as FeO): (a) and (b) show a comparison between all glass shard analyses for the TVC and MgVC sourced tephras; (c) and (d) indicate the distinction in glass compositional signature for the eruptives from the OVC and TVC that post-date the Kawakawa/Oruanui (KOT) eruption; (e) and (f) plots distinguish the glass analyses for tephra from the OVC into component eruptive time periods, with tephra from the Mangaone subgroup (Jurado-Chichay and Walker, 2000; Smith et al., 2002) distinguishable from all other tephra from the OVC; (g) and (h) show the similarity in the geochemical compositions of glass of the tephras from the OVC and TVC for the eruptions prior to, and including, the KOT eruption. Colours are consistent for each caldera source; symbols are representative of different groups of tephra defined in the keys for each set of plots.

4.1.2 Source-specific major and trace elements

The central TVZ contains nine recognised calderas, each with different eruption histories, but all having produced large magnitude/volume tephra-producing rhyolitic eruptives. Some of the calderas are attributed to single caldera collapse events (Rotorua, Reporoa, and Ohakuri), whereas others represent composite collapse events that overlap spatially but not temporally (Mangakino and Kapenga). However, the majority reflect multiple collapse events over an extended period of time (Maroa, Okataina, Taupō, and Whakamaru) (**Fig. 1**; Wilson et al., 1995a, 2009; Barker et al., 2021). Although the calderas are mostly discrete in space, evidence from multiple eruptions has shown their plumbing systems may be linked tectonically (e.g. Wilson et al., 2009; Allan et al., 2012). Hence, the ability to trace a tephra deposit to a caldera source through glass-shard geochemistry alone could be challenging.

The results of the PCA analysis suggest that tephra sourced from the TVC can be distinguished from those of a proposed Mangakino source (MgVC) (**Fig. 9**). Using SiO_2/K_2O vs. Na_2O+K_2O, the glass shards of the TVC tephras generally have higher SiO_2/K_2O and lower Na_2O+K_2O in comparison to those of the equivalent oxides for MgVC-sourced tephra (**Fig. 11a**). This information is important, but because of the large age differences for the calderas (TVC ~ 0.32 Ma to present, and MgVC ~1.6 Ma to 1.53 Ma and ~1.2 Ma to 0.95 Ma), the use of this distinction is likely more important for discussions on mantle source dynamics rather than for geochemical correlation of tephra deposits.

Previous studies have suggested that the geochemical characteristics of glass shards from TVC and OVC tephra deposits post-dating the eruption of the Kawakawa/Oruanui (KOT) can be distinguished using fO_2 of Fe-Ti oxides and minerals (Shane, 1998), pumice and lava compositions (Sutton et al., 2000), and glass chemistry (Stokes et al., 1992). Our results also show there is a bimodality in the TVC glass-shard data as a whole and that the post-KOT tephra deposits from the TVC and OVC are quite different whereas the pre-KOT tephra from OVC and TVC are similar (**Fig. 11c&d**). Most glass shards erupted after the KOT event from the TVC have low SiO_2 (≤ 77 wt.%) and less variable K_2O (~3 wt.%), and higher values for all other major elements in comparison with those of the glass shards erupted from the OVC (**Fig. 11c&d**). In contrast, tephra erupted from the TVC and OVC prior to, and including the KOT, do show a large amount of overlap in their glass geochemical signatures. For OVC (**Fig. 11 3&f**), there is a high density of samples that have their SiO_2

27

concentrations at ~78 wt.%; however, there is a high variability in SiO_2 overall, with Maketu, Hauparu, and Ngamotu of the Mangaone subgroup plotting with SiO_2 concentrations ≤~76 wt.%, and the remaining Mangaone subgroup samples (Unit L, Awakeri, and Mangaone) clustering at SiO_2 = 76–77.5 wt.% (FeO = ~1.2 wt.%, K_2O = ~2.8 wt.%, Al_2O_3 = ~13 wt.%, CaO = ~1.2 wt.%), a finding consistent with those of Smith et al. (2005) who divided the Mangaone subgroup into 'old' and 'young' eruptives on the basis of low and high SiO_2, respectively, unlike the other OVC sourced samples that plot around SiO_2 = ~77.5-79 wt.%, (FeO = ~0.8-0.9 wt.%, K_2O = 2.75-4.5 wt.%, Al_2O_3 = ~12-13 wt.%, CaO = ~0.5-1.0 wt.%; **Fig. 11c&d**). Analyses from the Rotoehu/Rotoiti tephra deposits plot independently from those of other OVC eruptives for this time period. However, they overlap with those of some TVC-tephra-derived glass compositions (Poihipi, Tahuna, Okaia, and KOT). The Rotoehu/Rotoiti tephra deposits have a markedly homogeneous geochemical signature and are also much older than TVC eruptions (**Table 1**). Hence, coupled with the thickness of the deposits, it is likely that a tephra linked to the Rotoehu/Rotoiti eruption would be obvious to distinguish through stratigraphic relationships and age combined with the geochemistry.

The TephraNZ dataset presented here also includes analyses of glass of samples from tephras erupted from the Kapenga Volcanic Centre (KVC; Earthquake Flat eruption), Rotorua Volcanic Centre (RoVC; Ararata Gully and Kakariki), and Whakamaru Volcanic Centre (WVC; Fordell, Upper and Lower Griffins Road, Potaka, Rewa, Pakihikura, and Mangapipi). In addition, some older tephra deposits have been recorded in the Whanganui Basin and elsewhere. These are well-known beds but their caldera sources are not yet defined (Alloway et al., 1993; Pillans et al., 1994, 2005; Shane et al., 1996; Rees et al., 2018, 2019, 2020). **Figure 12** shows a plot for the data from KVC, RoVC, and WVC with those regions populated by glass data from samples from the OVC, TVC and MgVC sources. Overall, the samples plot with a lower SiO_2/K_2O ratio (≤ ~25) similar to that of the MgVC-sourced tephra, which seems to be indicative of samples from older sources in comparison with those from the OVC and TVC. The samples potentially linked to RoVC (Bussell, 1986; Bussell and Pillans, 1997) show different geochemical compositions. For example, Kakariki-tephra-derived glass has slightly higher SiO_2 ≥ 78 wt.%) in comparison to that of the Ararata Gully tephra (SiO_2 ≤ 77wt %), suggesting that they are likely derived from different eruptions, but potentially the same source (Mamaku Ignimbrite reportedly has variable geochemical phases; Milner et al., 2003). Glass from the KVC sample (Earthquake Flat tephra) has a very homogeneous signature in the major elements, but a more variable signature in the trace elements, both of which overlap with OVC- and TVC-source signatures. There is a very large spread for the data from the unknown samples, precluding the ability to specify their source based simply on major and trace elements alone. Nevertheless, their glass compositional signatures are more similar to those of the older MgVC sourced tephra, in comparison to those of the younger TVC and OVC deposits, as would be expected based on their known age range (**Table 1**).
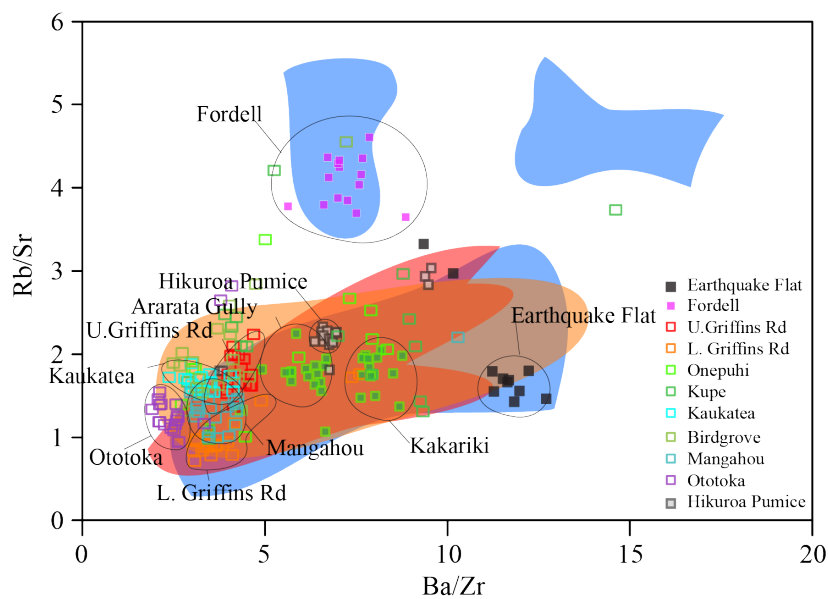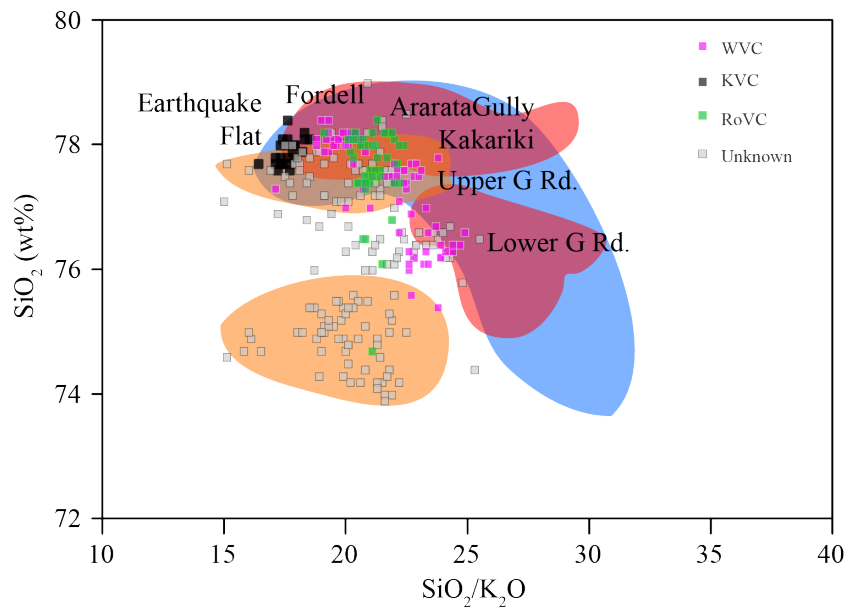
Figure 12. Major and trace element biplots of indicative elements in glass to show the relationships between the tephras from Mangakino Volcanic Centre (MgVC – orange shaded regions), Taupō Volcanic Centre (TVC – red shaded regions), and Okataina Volcanic Centre (OVC – blue shaded regions), and the tephras from known and unknown sources within the TephraNZ data base.

640

4.1.3 Homogeneous, heterogeneous, and bimodal samples

645   Fingerprinting of glass shards for correlation relies on the ability to distinguish between different deposits and therefore a homogeneous signature for a single eruptive that is distinct from all other samples is the ideal 'fingerprint'. However, sometimes there is more complexity in the geochemical data and heterogeneity can develop in a tephra deposit through a number of mechanisms including the following (Lowe, 2011):

650   (1) Variability in the magma body itself (e.g. Nairn, 1992; Nairn et al., 2004; Smith et al., 2004; Kobayashi et al., 2005; Shane et al., 2008; Charlier and Wilson, 2010; Klemetti et al., 2011; Cole et al., 2014);

(2) Proximal versus distal complexity, linked to (1) (e.g. Manning, 1996; Shane et al., 2003a; Holt et al., 2011);

655   (3) Post- or syn- depositional reworking (e.g. Schneider et al., 2001)

For example, the heterogeneous signature identified for glass from the Kaharoa tephra agrees with previous findings for this eruptive. Nairn et al. (2004) and Sahetapy-Engel et al. (2014) reported that glass compositional variability within the Kaharoa deposits shows sequential tapping of a stratified

660   magma body coupled with syn-eruptive changes in dispersal patterns. In general, this is likely one of the reasons why some of the proximal tephra deposits analysed in this study have a more variable geochemical signature in comparison to those of their distal counterparts (**Fig. 7**). Although the proximal deposits record the detail in the eruption progression, the distal deposits tend to record the very largest phase of the eruption (e.g. Walker, 1980), but differences can be expected to occur also

665   according to the azimuths of wind direction during an eruption and the number and degree of interconnectedness of magma bodies involved in the eruption (e.g. Walker, 1981; Kilgour and Smith, 2008; Sahetapy-Engel et al., 2014; Storm et al. 2014; Rubin et al., 2016).

The tephrochronological principle is much more likely to utilise distal unknown deposits, and therefore we suggest that using the distal signature (or signatures) maybe more appropriate for

670   correlation in many studies. In general, distal tephras are more chemically homogeneous – but with some notable and well-documented exceptions – and this attribute therefore allows them to be traced over large areas (Manning, 1996). Alternatively, the identification of heterogeneity or bimodality in distal tephras, once recognised, can be an additional useful characteristic for fingerprinting (e.g. Shane et al., 2003a, 2008; Lowe et al., 2017). These statements, however, rely on the tephra being identified as

675   a primary deposit, and not reworked. Reworking is commonly seen in paleofluvial deposits, for example those in the Whanganui Basin, and in other environments thin tephras are prone to mixing such as in surficial soils. This reworking can mix tephra from multiple eruptions, and can cause highly variable glass chemistry within a single deposit (e.g. Shane et al., 2005, 2006). Fluvial reworking can be commonly identified by sedimentary structures within the deposit, for example, ripples or cross bedding

680   indicative of fluvial transport and deposition (e.g. Shane, 1994; Schneider et al., 2001), over thickening of deposits (e.g. Vucetich and Pullar, 1969; Lowe, 2011), or through shard morphology, for example anomalously large shards or rounding of shards (e.g. Leaphy, 1997).

Heterogeneous signatures (defined in approximation of where the standard deviation of the analyses is greater than the analytical error) in major element compositions were identified for ten of the
685   tephra deposits: Kaharoa, Taupō Y5 proximal (P), Whakatane P, Hauparu, Maketu, Ngamotu, Fordell, Onepuhi, Birdgrove, and Ototoka. Our data show that for some samples, specific trace elements and trace element ratios have lower geochemical variability (**Fig. 13a**). The elements that work best to separate out the individual units within a deposit with a heterogeneous signature reflect the minerals that have formed during fractional crystallisation of the melt. Because of this, different elements or element
690   ratios work for different tephras. For example, for glass from Kaharoa, Sr exhibits little variability (27–79 ppm), whereas for glass from Taupō, Sr compositional range exemplifies the heterogeneity in the sample (62–158 ppm; **Fig. 13a**).

Bimodality was identified for glass shards derived from four of the tephra horizons analysed: Rotorua (OVC), Rerewhakaaitu (OVC), Poihipi (TVC), and Tahuna (TVC). For all four of these, K_2O
695   concentration in glass exhibits bimodality, and therefore trace elements with similar chemical properties reinforce the bimodality (for example, LILEs Rb, Sr, and Cs; HFSEs Zr, or REE Eu), whereas most other trace elements do not show this bimodal signature (**Fig. 13b**).

4.2. Indistinguishable tephras

Euclidean similarity coefficient (ESC) analysis was used on all glass-shard reference data for
700   tephras from Rotoiti/Rotoehu to Kaharoa in addition to the PCA and geochemical investigation to determine those samples that have indistinguishable element concentrations at similar ages (**Fig. 14**). **Figure 14** shows that similarities (similarity coefficient values (SC)) are observed in the major element signatures of glass analyses for the following tephras: Waimihia and Unit K (SC = 0.11); Rotoma-P and Whakatane-D (SC = 0.18); Mamaku and Rotoma-P, -D (SC = 0.19 and 0.2, respectively); Poihipi and
705   Rotoma-P (SC = 0.18); Rotoiti/ Rotoehu and Rotoma-D (SC = 0.13); Te Rere and Rerewhakaaitu (SC = 0.16); Tahuna and Rotoma-P (SC = 0.19); KOT and Okaia (SC = 0.11); KOT and Unit L (SC = 0.21); and Poihipi and Tahuna (SC = 0.18). When the key trace element are analysed (of the eruptions identified as having similar major elements), Waimihia and Unit K (SC = 8.88), Whakatane and Rotoma (SC = 7.79), Poihipi and Tahuna (SC = 4.24), KOT and Okaia (SC = 4.25), and KOT and Unit
710   L (SC = 8.44) come up with significantly low (<10) similarity coefficients for trace elements also, hence suggesting these samples will be indistinguishable in both major and trace elements. In addition, when simple geochemical assessment is applied, similarities are observed between glass analyses for Taupō and Waimihia; Mamaku and Rotoma-D; and Waiohau, Rotorua, and Rerewhakaaitu (**Table 4**).

Table 4 outlines the key eruptions that show similar geochemical signatures in their glass chemistry,
715 and the ways in which they can be distinguished.

Figure 15a shows that for Poihipi and Tahuna the best separation (although some overlap remains) is seen in the ratios La/Yb vs. Ba/Y; in addition, Tahuna also shows a bimodality in Ba/Th ratio which is not seen for Poihipi. For Rotoma and Mamaku, the tephras can be separated (although some overlap remains) using Ba/Th vs. Rb/Sr and Rb/Zr vs. Rb/Sr (**Fig. 15b**). Rotoma and
720 Rotoehu/Rotoiti are very similar in their glass-shard major elements though can be distinguished using specific, but a wide range of, trace elements (**Fig. 15c**). They are also very different in age, hence should not be too difficult to distinguish on the basis of stratigraphic positioning or dating.

Waimihia and Unit K (Taupō Subgroup) tephras are very difficult to distinguish, and their similar late- to mid-Holocene ages (3382 ± 50 and 5088 ± 73 cal. yr BP, respectively; Lowe et al.,
725 2013) and mineralogy could see them misidentified if dates were unavailable or imprecise. Geochemical investigation beyond the PCA and SC analyses of glass shows that Lu, Sc, Mn, and Co can be used to geochemically distinguish these two tephras (**Fig. 15d**), indicative of fractional crystallisation of differing amounts of clinopyroxene, plagioclase, and amphibole during the eruptive events. Although not identified by the SC analysis directly, Poronui ($11,195 \pm 51$ cal yr BP) and
730 Karapiti ($11,501 \pm 104$ cal. yr BP) tephras also have comparable age, geochemistry, and mineralogy; thus using major, trace, and trace element ratios these two tephras remain indistinguishable. Glass shards from the three Holocene tephras, Waimihia, Poronui, and Karapiti, also have very similar trace element and trace-element ratios but, as for Waimihia and Unit K, they can be distinguished with Lu, Sc, Mn, and Co, where Waimihia has higher Sc, Lu, and Mn, but lower Co in comparison to those of
735 the Poronui and Karapiti tephras. They can also be distinguished simply with a biplot of FeO vs. CaO, or Na_2O+K_2O or SiO_2/K_2O, or SiO_2, where the Waimihia samples in general have lower FeO, Na_2O+K_2O, SiO_2/K_2O, and higher CaO, and SiO_2 in comparison to the equivalent values for Poronui and Karapiti samples (**Fig. 15e, Table 4**).

Geochemical investigation and PCA also highlight the similarity of the glasses of Waiohau,
740 Rotorua, and Rerewhakaaitu tephras. There is added complexity with these samples as we have both proximal and distal deposits to compare, where, as discussed previously, the proximal samples will likely be more heterogeneous. Glass analyses of the Waiohau tephra show it can be distinguished from those for the Rotorua and Rerewhakaaitu tephras using a range of trace elements and trace-element ratios. In addition, the Rotorua and Rerewhakaaitu tephras are observed to be bimodal for some
745 elements. The Waiohau also has different mineralogy from that of Rotorua and Rerewhakaaitu tephras (Froggatt and Lowe, 1990; Lowe et al., 2008). Conversely, the Rotorua and Rerewhakaaitu tephras are indistinguishable in geochemistry and mineralogy, and therefore accurate dating and stratigraphic super-positioning would have to be relied upon to distinguish them with certainty (**Fig. 15f, Table 4**).
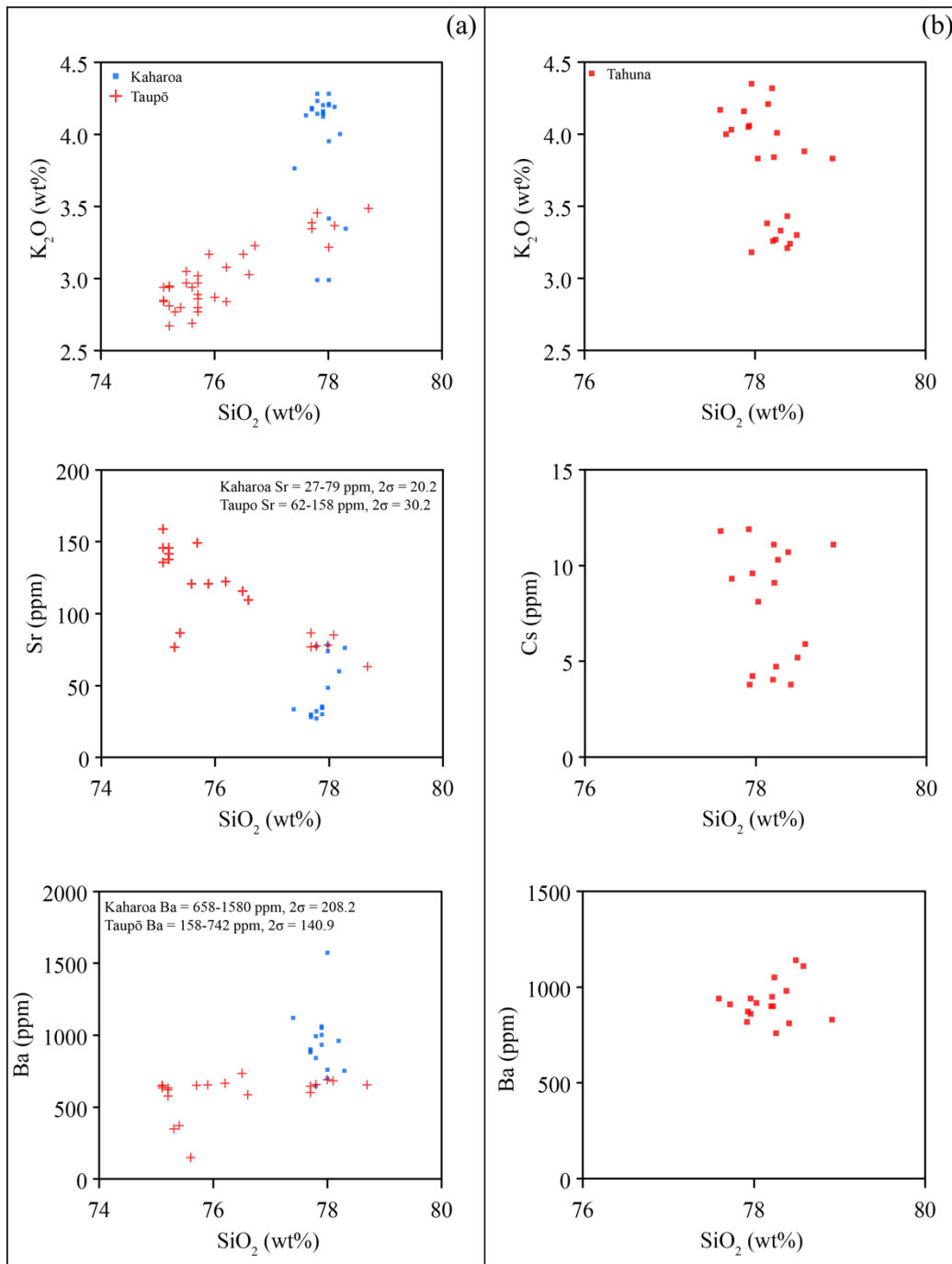
Figure 13. Biplots to show examples of how trace elements in glass enable manipulation of heterogeneous and bimodal geochemical data. Panel (a) shows analyses of glass from Kaharoa and Taupō tephras, both of which show a heterogeneous signature with most major elements (presented on a normalised basis). Sr has a low variability for Taupō, but does not for Kaharoa tephra; conversely, Ba has a low variability for Kaharoa, but does not for Taupō. Panel (b) shows the bimodal signature created for Tahuna tephra using K₂O composition; this is also seen for Cs but not for Ba.

(a)

	Kaharoa	Taupo	Waimihia	Unit K	Whakatane-D	Whakatane-P	Mamaku	Rotoma-P	Rotoma-D	Opepe	Poronui	Karapiti	Waiohau-P	Waiohau-D	Rotorua-P	Rotorua-D	Rerewhakaaitu-P	Rerewhakaaitu-D	Okareka	Te Rere	KOT	Poihipi	Okaia	Unit L	Awakeri	Mangaone	Hauparu	Maketu	Nga Motu	Tahuna	EQF	Rotoehu	Rotoiti
Kaharoa	0.00																																
Taupo	2.40	0.00																															
Waimihia	2.31	0.21	0.00																														
Unit K	2.21	0.25	0.11	0.00																													
Whakatane-D	0.50	2.75	2.64	2.56	0.00																												
Whakatane-P	1.05	1.56	1.44	1.36	1.25	0.00																											
Mamaku	0.59	2.63	2.51	2.43	0.27	1.11	0.00																										
Rotoma-P	0.43	2.58	2.48	2.39	0.18	1.08	0.19	0.00																									
Rotoma-D	0.63	2.52	2.39	2.31	0.44	1.00	0.20	0.30	0.00																								
Opepe	2.61	0.48	0.55	0.61	2.94	1.77	2.81	2.78	2.70	0.00																							
Poronui	1.98	0.55	0.48	0.43	2.30	1.12	2.17	2.14	2.06	0.65	0.00																						
Karapiti	1.76	0.76	0.69	0.63	2.08	0.93	1.96	1.92	1.86	0.87	0.24	0.00																					
Waiohau-P	0.72	2.30	2.16	2.08	0.69	0.81	0.48	0.52	0.30	2.51	1.87	1.68	0.00																				
Waiohau-D	0.87	2.39	2.25	2.17	0.74	0.89	0.54	0.60	0.37	2.60	1.97	1.76	0.20	0.00																			
Rotorua-P	0.70	1.87	1.77	1.68	0.90	0.41	0.79	0.74	0.71	2.09	1.44	1.23	0.55	0.66	0.00																		
Rotorua-D	0.41	2.20	2.14	2.04	0.85	1.03	0.94	0.78	0.96	2.46	1.84	1.63	0.95	1.09	0.71	0.00																	
Rerewhakaaitu-P	0.42	2.51	2.41	2.32	0.37	1.04	0.47	0.32	0.55	2.73	2.09	1.86	0.65	0.71	0.67	0.61	0.00																
Rerewhakaaitu-D	0.27	2.20	2.12	2.02	0.67	0.89	0.72	0.57	0.74	2.42	1.79	1.57	0.74	0.89	0.53	0.25	0.44	0.00															
Okareka	0.98	2.75	2.61	2.53	0.64	1.23	0.41	0.59	0.38	2.89	2.27	2.07	0.57	0.53	1.00	1.32	0.84	1.09	0.00														
Te Rere	0.42	2.57	2.48	2.39	0.34	1.11	0.49	0.33	0.60	2.79	2.15	1.93	0.73	0.79	0.77	0.64	0.16	0.49	0.87	0.00													
KOT	0.97	1.99	1.86	1.79	0.99	0.52	0.80	0.84	0.72	2.11	1.49	1.29	0.63	0.63	0.49	1.12	0.89	0.89	0.83	0.96	0.00												
Poihipi	0.43	2.43	2.33	2.24	0.33	0.93	0.26	0.18	0.31	2.63	1.98	1.76	0.46	0.55	0.58	0.73	0.29	0.50	0.61	0.35	0.69	0.00											
Okaia	1.07	1.96	1.83	1.76	1.08	0.53	0.88	0.94	0.79	2.08	1.46	1.27	0.69	0.73	0.57	1.22	0.99	0.99	0.87	1.06	0.21	0.78	0.00										
Unit L	0.91	1.98	1.85	1.77	0.95	0.48	0.74	0.79	0.62	2.14	1.51	1.32	0.47	0.53	0.42	1.07	0.86	0.84	0.77	0.94	0.21	0.64	0.25	0.00									
Awakeri	1.23	1.56	1.40	1.33	1.44	0.53	1.24	1.26	1.08	1.73	1.13	1.00	0.95	1.01	0.86	1.40	1.20	1.26	1.40	0.72	1.13	0.69	1.40	0.78	0.00								
Mangaone	1.82	0.96	0.81	0.75	2.14	1.07	1.97	1.96	1.83	1.09	0.66	0.69	1.61	1.73	1.34	1.76	1.98	1.69	2.03	2.06	1.40	1.83	1.37	1.34	0.78	0.00							
Hauparu	1.33	1.06	1.20	1.27	3.68	2.54	3.56	3.53	3.46	0.81	1.42	1.63	3.26	3.36	2.84	3.14	3.47	3.13	3.66	3.54	2.89	3.38	2.86	2.91	2.47	1.75	0.00						
Maketu	5.47	3.17	3.32	3.39	5.87	4.72	5.76	5.71	5.65	3.01	3.62	3.83	5.44	5.54	5.02	5.32	5.63	5.27	5.87	5.69	5.11	5.56	5.07	5.12	4.65	3.91	2.33	0.00					
Nga Motu	2.95	0.87	0.94	1.00	3.29	2.17	3.15	3.13	3.04	0.57	1.08	1.30	2.84	2.95	2.46	2.80	3.11	2.78	3.11	3.22	3.18	2.49	2.50	2.02	1.29	0.54	2.09	5.69	0.00				
Tahuna	0.49	2.57	2.47	2.38	0.23	1.07	0.27	0.19	0.41	2.75	2.11	1.89	0.61	0.67	0.73	0.79	0.28	0.57	0.63	0.30	0.79	0.18	0.89	0.78	1.30	1.99	3.53	5.69	3.12	0.00			
EQF	0.72	2.72	2.67	2.57	0.81	1.46	1.01	0.87	1.16	2.90	2.30	2.06	1.30	1.39	1.15	0.74	0.71	0.72	1.38	0.65	1.34	0.87	1.44	1.38	1.79	2.32	3.60	5.70	3.28	0.77	0.00		
Rotoehu	0.72	2.59	2.46	2.38	0.45	1.06	0.19	0.34	0.13	2.77	2.13	1.93	0.38	0.39	0.78	1.06	0.59	0.83	0.27	0.63	0.73	0.36	0.80	0.65	1.15	1.91	3.53	5.73	3.11	0.41	1.18	0.00	
Rotoiti	0.76	2.56	2.43	2.35	0.51	1.04	0.25	0.39	0.13	2.74	2.10	1.90	0.34	0.35	0.77	1.08	0.63	0.85	0.26	0.68	0.71	0.40	0.77	0.62	1.11	1.87	3.50	5.70	3.08	0.47	1.23	0.07	0.00

(b)

	Kaharoa	Taupo	Waimihia	Unit K	Whakatane-P	Mamaku	Rotoma	Opepe	Poronui	Karapiti	Waiohau-P	Waiohau-D	Rotorua-P	Rotorua-D	Rerewhakaaitu-P	Rerewhakaaitu-D	Okareka	Te Rere	KOT	Poihipi	Okaia	Unit L	Awakeri	Mangaone	Hauparu	Maketu	Nga Motu	Tahuna	EQF	Rotoehu	Rotoiti
Kaharoa	0.00																														
Taupo	25.7	0.00																													
Waimihia	33.7	9.19	0.00																												
Unit K	25.2	6.36	8.88	0.00																											
Whakatane-P	14.4	13.6	20.0	11.2	0.00																										
Mamaku	9.60	16.5	24.1	15.7	5.38	0.00																									
Rotoma	21.2	6.31	12.5	4.46	7.79	11.6	0.00																								
Opepe	14.7	13.8	20.2	11.6	3.46	6.29	8.27	0.00																							
Poronui	11.7	18.2	24.4	15.6	5.12	5.59	12.4	4.86	0.00																						
Karapiti	27.8	6.18	6.55	3.71	14.1	18.3	6.83	14.0	18.2	0.00																					
Waiohau-P	25.6	1.23	9.82	7.36	14.0	16.6	6.86	14.1	18.5	6.99	0.00																				
Waiohau-D	24.0	2.06	11.0	7.02	12.4	14.9	5.58	12.5	16.9	7.19	1.73	0.00																			
Rotorua-P	20.3	5.96	14.4	8.29	11.4	14.4	4.76	9.17	13.6	9.18	5.74	4.09	0.00																		
Rotorua-D	12.8	38.4	46.3	37.8	26.7	22.2	33.8	26.9	23.1	40.3	38.4	36.7	33.0	0.00																	
Rerewhakaaitu-P	1.36	26.2	34.2	25.8	15.0	10.2	21.7	15.1	12.1	28.3	26.1	24.4	20.7	12.3	0.00																
Rerewhakaaitu-D	3.43	28.3	36.3	28.0	17.3	12.3	23.8	17.6	14.4	30.4	28.1	26.5	22.8	10.3	2.90	0.00															
Okareka	3.72	12.2	7.40	11.5	13.7	5.95	11.3	15.7	7.64	3.39	1.83	2.56	35.4	23.2	25.2	27.8	0.00														
Te Rere	10.0	30.4	36.7	27.9	17.0	14.6	24.7	17.3	12.6	30.7	30.7	29.0	25.5	13.7	10.2	10.8	27.8	0.00													
KOT	12.5	13.7	22.1	14.5	7.42	4.93	10.1	7.02	9.07	16.4	13.5	11.8	8.04	25.1	12.8	14.9	10.4	19.0	0.00												
Poihipi	3.23	24.2	31.7	23.2	12.2	7.73	19.2	12.6	9.06	25.7	24.2	22.5	18.9	14.6	3.69	5.49	21.3	8.69	11.4	0.00											
Okaia	8.58	17.7	25.8	16.3	8.25	3.62	13.4	7.76	7.42	19.8	17.6	15.9	12.1	32.7	20.5	22.6	3.98	24.3	15.1	4.25	0.00										
Unit L	20.1	6.48	13.8	6.38	7.73	10.6	2.23	7.79	12.0	8.02	6.72	5.13	2.93	32.7	20.5	22.6	3.98	24.3	14.5	18.3	12.0	0.00									
Awakeri	34.3	11.1	3.15	9.08	20.2	24.7	13.2	20.3	24.3	7.07	11.9	12.9	15.7	46.8	34.8	37.0	13.9	36.5	32.2	26.5	14.8	23.1	0.00								
Mangaone	48.3	22.9	14.9	23.8	34.9	38.9	27.4	34.9	39.2	21.1	23.2	24.7	28.4	61.1	48.8	50.9	26.0	51.6	36.4	46.5	40.2	28.4	15.3	0.00							
Hauparu	56.9	32.2	25.6	33.7	44.3	47.8	36.8	43.4	48.0	30.5	32.2	33.6	36.8	69.4	57.2	59.4	34.6	60.5	44.6	55.3	48.4	37.3	25.8	13.3	0.00						
Maketu	58.9	34.6	27.1	35.0	45.7	49.8	38.6	44.9	49.3	32.0	34.8	36.2	39.2	71.4	59.3	61.6	37.2	61.6	47.0	57.1	50.6	39.4	26.5	14.7	1.77	0.00					
Nga Motu	66.0	41.6	35.5	43.5	53.8	57.2	46.4	52.8	57.5	40.2	41.5	43.0	46.0	78.4	66.3	68.4	43.9	70.0	53.7	66.5	57.5	46.4	35.8	22.8	10.0	13.5	0.00				
Tahuna	2.47	26.1	34.2	25.9	15.4	10.3	21.7	15.4	12.6	28.2	26.0	24.3	20.6	12.5	1.74	2.51	23.0	11.2	12.6	4.24	8.69	20.5	34.9	48.8	57.1	59.3	66.1	0.00			
EQF	14.4	11.6	19.9	12.4	6.56	5.78	7.96	6.58	9.47	14.2	11.4	9.73	6.06	27.0	14.8	16.8	8.39	20.3	2.35	13.0	6.28	6.27	21.0	34.2	42.8	45.1	52.0	14.6	0.00		
Rotoehu	35.6	10.3	6.25	13.0	23.1	26.4	15.4	22.8	27.4	9.99	10.3	11.9	15.3	48.5	36.1	38.1	13.0	39.9	23.3	34.0	27.3	15.9	8.65	13.5	22.0	24.9	31.5	35.9	21.3	0.00	
Rotoiti	31.7	6.34	6.61	10.3	19.6	22.6	11.9	19.4	24.0	7.88	6.20	7.77	11.4	44.4	32.1	34.1	9.00	36.4	19.4	30.2	23.4	12.2	9.33	17.4	26.1	28.9	35.4	31.9	17.4	4.24	0.00

Figure 14. Results of Euclidean similarity coefficient (ESC) calculations for (a) major, and (b) trace element concentrations in glass from all the tephras analysed. See Supplementary Material 2 for R code used for these calculations. Colour coding shows ESC values: white shows the smaller the value (similar compositions) through to black showing the larger the values (different compositions). The lowest values (<0.2), and hence the most similar tephras compositionally (based on Al_2O_3, K_2O, SiO_2, Na_2O, TiO_2, **FeOt, and MnO major elements and V, Co, Rb, Nd, Eu, Yb, Th, and U trace elements) are highlighted with bold outlines and red text. Tephras from Taupō Volcanic Centre are shaded red, and those from Okataina Volcanic Centre are shaded blue.**

Figure 15. Biplots for glass analyses for specific tephras which have very similar compositions and similar ages (see text for discussion and Table 4 for alternative elements). Plots show examples of the elements in glass that enable these tephras to be separated: (a) Poihipi and Tahuna (from TVC); (b) Mamaku and Rotoma-D (from OVC; note no trace element data were obtained for Rotoma-P); (c) Rotoma and Rotoiti/Rotoehu (from OVC); (d) Waimihia and Unit K (from TVC); (e) Waimihia, Poronui and Karapiti – note that Poronui and Karapiti are indistinguishable using glass-chemistry; and (f) Waiohau, Rerewhakaaitu and Rotorua – note that Rerewhakaiatu and Rotorua are indistinguishable using glass chemistry. All major element data are presented on a normalised basis, and total iron is expressed as FeO.

770

775   KOT, Okaia, and Unit L (Mangaone Subgroup) show indistinguishable major elements in their constituent glass shards and very similar trace elements. The TephraNZ samples have been compared with existing published data and are complementary with the existing data with respect to major elements (e.g. Sandiford et al., 2002; Shane et al., 2002; Smith et al., 2002; 2005; Lowe et al., 2008; Allan et al., 2008; Molloy, 2008). This is the first time trace element glass data have been published for

780 Unit L and Okaia tephras. Our results show that Unit L glass shows bimodality in Rb/Zr, Ba/Th, Ce/Th and Y/Th and in this way, it can therefore be distinguished from the KOT and Okaia tephras (**Table 4**).

4.3. Proposed future research

        This foundation dataset, derived in a formalised way, is unique in New Zealand and provides

785 researchers with new avenues of research. It is our aim that the foundation dataset can be improved and expanded with analyses of other known deposits, and that a subsidiary catalogue of accurately correlated geochemical analyses for such deposits can be added to bolster the dataset. As noted earlier, it is beyond the scope of this paper to dive too deeply into the detail of the data, but we feel that it will provide the basis for countless projects in the future. Below we highlight some of the current gaps

790 which we think would benefit from further research.

4.3.1 Further statistical analysis

        We have applied simple ordination and statistical analyses to this dataset; however, we believe that further rigorous statistical analysis could be applied. Firstly, the analyses we present in this

795 publication have been applied to mean values for each of the tephra samples (e.g. data from **Table 2**); there is no reason why these simple tests could not be applied to the full dataset, using all the individual (shard by shard) values analysed for each sample. Secondly, we chose very basic tests (PCA and ESC) to fit with our requirements, but there is likely some more appropriate statistical test that could be applied to get the most out of this exceptional dataset. For example, (extended) canonical variates

800 analysis (CVA): by applying CVA to PCA results could determine optimal discrimination between multivariate data for single tephra deposits. This discrimination will increase the ability to identify an unknown tephra based on its similarity to known signatures plotted in multivariate space (e.g. discriminant function analysis; Tyron et al., 2009; 2010; Lowe et al., 2017; Bolton et al., 2020).

805 #### 4.3.2 Whanganui Basin correlatives

        A number of the tephras reported in this research were sampled from the Whanganui Basin, an uplifted Plio-Pleistocene basin margin sequence that preserves as many as 45-superposed cyclothems

deposited since ~3 Ma (Naish et al., 1996, 2005; Naish and Kamp, 1997; Carter and Naish, 1998; Carter
et al., 1999; Pillans, 2017; Grant et al., 2018, 2019; Tapia et al., 2019). The tephra deposits within the
basin contribute to the robust chronological framework that has been constructed for this region
(Seward, 1976; Beu and Edwards, 1984; Alloway et al., 1993; Naish and Kamp, 1995; Shane et al.,
1996; Saul et al., 1999; Pillans et al., 1994, 2005; Naish et al., 1996, 2005; Rees et al., 2018, 2019,
2020; Hopkins et al., 2021). These and other tephras (such as those derived from Tauranga Volcanic
Centre) also record a critical time in New Zealand's volcanological history – the transfer between
activity from the Coromandel Volcanic Zone to the Taupō Volcanic Zone (Briggs et al., 2005; Pittari et
al., 2021). Deposits from this period are generally poorly exposed at source, and thus distal tephras
could provide an insight into the eruptive history, geochemical evolution, and potentially even caldera
evolution during this period (Houghton et al., 1995; Pittari et al., 2021). Most of the tephras reported in
this research are well known and well dated, which is why they were included in the study. However,
most do not have a known source caldera or source eruptives, or have only been variably correlated to
other deposits in New Zealand (e.g. Lowe et al., 2001; Pearce et al., 2008). There are also numbers of
tephra deposits in the Whanganui Basin that have yet to be studied, and thus a research project that is
tephra focused, rather than using it as an accessory to a different line of enquiry, is timely.

4.3.3 IODP and ODP correlatives

At present there is a wealth of information that has yet to be fully investigated in the tephra
record of the ODP Leg 181 Sites 1122, 1123, 1124, 1125 (Carter et al., 2003, 2004; Alloway et al.,
2005; Allan et al., 2008) and IODP Expedition 372 and 375 sites U1517 and U1520 (Pecher et al.,
2018; Saffer et al., 2018). Pioneering work includes that undertaken by Watkins and Huang (1977) and
Nelson et al. (1985) and findings from more 'local' marine coring expeditions include those reported by
Shane et al. (2006). The new reference material built by this project will allow more definitive
identification and correlation of tephras within these cores, specifically post-2 Ma. However, the reports
currently published on these deposits suggest that there are many more tephra deposits to be found in
these marine and offshore sites than we have in the TephraNZ dataset (Carter et al., 2003; Alloway et
al., 2005; Holt et al., 2010, 2011; Hopkins et al., 2021). The TephraNZ dataset can provide a formalised
correlation framework from which other unknown deposits can be determined, characterised, and
integrated into a holistic tephrostratigraphic reconstruction. Allan (2008) and Allan et al. (2008)
reported the major and trace element geochemistry of glass shards for tephra deposits dating from ~1.65
Ma in the ODP 1123 core. They also give orbitally-tuned ages for these tephras. However, of the 38
identified tephras only seven were correlated to onshore equivalents. In addition, Alloway et al. (2005)
reported over 100 tephra layers in the four ODP Leg 181 cores, dating back through orbital tuning
(astrochronology) to 1.81 Ma. Using major element chemistry of constituent glass shards, 13 tephras

were correlated to equivalent onshore tephras including KOT, Omataroa, Rangitawa/Onepuhi, Kaukatea, Kidnappers-B and -A/Potaka, Unit D/Ahuroa, Ongatiti, Rewa, Sub-Rewa, Pakihikura, Ototoka, and Table Flat. Analyses of glass from some of these are currently not in the TephraNZ database but could be easily added if the appropriate reference samples were available along with the capacity to analyse them. Alloway et al. (2005) reported an additional six tephra deposits that are correlated between the cores, but not to onshore equivalents, leaving potentially ~81 tephra horizons within the ODP cores that are uncorrelated. The information that could derive from their analysis would provide many details about the timing and evolution of the TVZ eruptions that is currently unobtainable from onshore deposits.

4.3.4 Mineral compositions

The TephraNZ reference dataset is only populated by glass major and trace element analyses at present. This is because glass geochemistry is one of the most frequently used and accessible tools for tephra correlation. Aerodynamic sorting of tephra componentry through transportation adds to the favourability of glass shards as the dominant tool because glass shards tend to be the only phase that is found at both proximal and distal sites. However, previous New Zealand-based studies have specified how mineral assemblages and their geochemical compositions can be used to distinguish certain tephras and their source (e.g. Nairn and Kohn, 1973; Lowe, 1988; Froggatt and Lowe, 1990; Froggatt and Rogers, 1990; Shane, 1998; Shane et al., 2003b; Allan et al., 2008; Lowe et al., 2008; Lowe, 2011). For example, the mineral cummingtonite, where predominant, is a known identifier for tephras from the Haroharo complex of the OVC (Whakatane, Rotoma, Rotoehu/Rotoiti (**Table 3)**; Ewart, 1968; Lowe, 1988; Froggatt and Lowe, 1990). At present, ferromagnesian mineralogical assemblages (following Froggatt and Lowe, 1990; Smith et al., 2005; Lowe et al., 2008) for all the TephraNZ samples younger than and including Rotoehu/Rotoiti have been published (see **Table 3**). Extending this tabulation to include the older samples would add another useful criterion to the correlation toolbox for tephras containing ferromagnesian minerals.

Additionally, the fractional crystallisation of plagioclase, biotite, amphibole, zircon, hydrous mineral phases, or Fe-Ti oxides has been shown to be the key impactor on the trace element chemistry (Shane, 1998; Allan, 2008; Turner et al., 2009, 2011). Thus the prevalence of these minerals is also an important potential fingerprinting tool. The information on the mineralogy of the tephras is not only useful for fingerprinting but also can be used in determining the characteristics of the magma source components, and potentially provide estimates for the temperature, pressure, and oxidation states of the magmatic system before eruption (e.g. Lowe, 1988, 2011; Shane, 1998). Thus, this information can allow hypotheses to be developed on the reactivation and triggering of these large-scale eruptions, an important step for hazard and risk monitoring.

4.3.5 The New Zealand tephra "Bermuda Triangle"

At present the TephraNZ database is very well populated for samples from the Rotoiti/Rotoehu through to Kaharoa eruption. It also has a high number of samples, but not an exhaustive list, from Mamaku ignimbrite (~0.22–0.23 ka) to the Hikuroa Pumice (2 Ma). There is a stark deficit in tephras between the Rotoiti/Rotoehu eruption and Mamaku ignimbrite (**Table 1**). This ~150 kyr gap in the volcanic record (~220 ka to 45 ka) is intriguing as there is proximal evidence for activity during this period. For example, Rosenberg et al. (2020) reported the occurrence of volcanic formations in cores form the Taupō region in the age range of ~168 to 92 ka, including the Huka Falls formations, Racetrack rhyolites, and the Te Mihi rhyolites. Tephra deposits, in some cases strongly weathered successions of multiple units broadly lumped together as a 'formation', such as the so-called Hamilton Ash Formation, have been reported during this time period both terrestrially and in marine and lacustrine sediment cores (Ward, 1967; Pain, 1975; Vucetich et al., 1978; Iso et al., 1982; Froggatt, 1983; Manning, 1996; Lowe et al., 2001; Newnham et al., 2004; Allan et al., 2008; Briggs et al., 2006; Lowe, 2019; B. Laeuchli *pers. comms.* 2020). However, at present the authors are not aware of a detailed, up-to-date study into the primary compositions of these tephra deposits. The key deposits identified during this time period include (but are not limited to) Kaingaroa Ignimbrite (~0.18 Ma; Froggatt, 1983), Tablelands Tephra Formation (~0.21–0.18 Ma; Iso et al., 1982, 0.39-0.34 Ma; Manning, 1996), Hamilton Ash Formation (0.34–0.125 Ma; Lowe, 2019); Kutarere tephra (= Mamaku ignimbrite 0.22–0.23 Ma; Shane et al., 1994; Houghton et al., 1995; Black et al., 1996; Tanaka et al., 1996; Milner et al., 2003), Kukumoa Subgroup (~0.22–0.05 Ma; Manning, 1996), and Tikotiko Ash (~0.125 ka; Lowe, 2019). A number of these studies are outdated, and with improved methodologies (major and trace element analysis, potentially of melt inclusions where preserved, dating techniques, and other measures to help construct time frames such as via phytolith studies to determine glacial vs interglacial periods, and potentially also paleomagnetic measures as shown for the much older and very strongly weathered Kauroa Ash Formation: Hopkins et al., 2021) it could be timely to further investigate this period of (apparent) deficit.

5. Conclusions

Major and trace element geochemical compositions of glass shards for a large suite of prominent, widespread New Zealand rhyolitic tephras have been analysed systematically and published for the first time as "TephraNZ". TephraNZ is a foundation dataset for collating geochemical data about New Zealand tephras based on analyses of their glass components. The foundation reference dataset is made up of known deposits that have their ages quantified through independent methods, and/or are from the type sites where tephras were first defined, or well-documented reference sections. Detailed methodology is reported to allow subsequent research to acquire comparable data to those in this

database. Principal component analysis of the glass geochemistry indicates that for the TephraNZ foundation dataset, as a whole, major elements Al, K, Si, Ti, Fe, Mn, and Cl are responsible for the spread along PC1 and PC2 space. When the trace elements are run together with the major elements, V, Co, Mg, Cu, Ti, Sr, Sc, Ca, Cs, Zr, Th, Rb, are most responsible for the separation in PC1 and PC2 space. Euclidean similarity coefficients can also be used to distinguish between some geochemically similar glass analyses. However, further detailed geochemical investigation is required to distinguish others. Geochemically indistinguishable tephras (on the basis of both major and trace element glass-shard compositions) are identified as Taupō and Waimihia; Poronui and Karapiti; Rotorua and Rerewhakaaitu; and KOT and Okaia. Only Poronui and Karapiti are noted as entirely indistinguishable, with other methods of characterisation listed as alternative options, including mineralogy, age, and stratigraphic relationships.

6. Author contribution

JLH and RJW designed the project. DJL and BJP contributed samples from previous field campaigns, and DJL provided guidance on new and existing field locations for sample collection. JLH and JEB undertook the field work, lab work, analysis and data reduction. ABHR advised on statistical analysis and R-coding. LA supervised and helped JEB develop LA-ICP-MS analysis and data reduction. FT supervised and helped JEB develop sample mounting and polishing procedures. JLH wrote the manuscript with contributions from all co-authors.

7. Competing interest

The authors declare that they have no conflict of interest.

8. Acknowledgements

9. Data Transparency

All the data provided by this manuscript can be downloaded as excel files from *Geochronology*. The data are also available from GNS Science, New Zealand, at Pet Lab (https://pet.gns.cri.nz), on TephraNZ website (www.tephranz.com), and as a file submission on EarthChem.

9. References

Abbott, P., Bonadonna, C., Bursik, M., Cashman, K., Davies, S., Jensen, B., Kuehn, S., Kurbatov, A., Lane, C., Plunkett, G., Smith, V., Thomlinson, E., Thordarsson, T., Walker, D.J., Wallace, K., 2021. Community Established Best Practice Recommendations for Tephra Studies-from Collection through Analysis (Version 3.0.0) [Data set]. Zenodo. http://doi.org/10.5281/zenodo.5047775

Allan, A.S., 2008. An elemental and isotopic investigation of Quaternary silicic Taupo Volcanic Zone tephras from ODP Site 1123: chronostratigraphic and petrogenetic applications. MSc thesis, Victoria University of Wellington, Wellington, New Zealand.

Allan, A.S., Baker, J.A., Carter, L. and Wysoczanksi, R.J., 2008. Reconstructing the Quaternary evolution of the world's most active silicic volcanic system: insights from an~ 1.65 Ma deep ocean tephra record sourced from Taupo Volcanic Zone, New Zealand. Quaternary Science Reviews, 27(25-26), pp.2341-2360.

Allan, A.S.R., Wilson, C.J.N., Millet, M.-A. and Wysoczanski, R.J., 2012. The invisible hand: tectonic triggering and modulation of a rhyolitic supereruption. Geology, 40, pp.563-566.

Alloway, B.V., Pillans, B.J., Sandhu, A.S. and Westgate, J.A., 1993. Revision of the marine chronology in the Wanganui Basin, New Zealand, based on the isothermal plateau fission-track dating of tephra horizons. Sedimentary Geology, 82(1-4), pp.299-310.

Alloway, B.V., Pillans, B.J., Carter, L., Naish, T.R. and Westgate, J.A., 2005. Onshore–offshore correlation of Pleistocene rhyolitic eruptions from New Zealand: implications for TVZ eruptive history and paleoenvironmental construction. Quaternary Science Reviews, 24(14-15), pp.1601-1622.

Alloway, B.V., Lowe, D.J., Larsen, G., Shane, P.A.R. and Westgate, J.A., 2013. Tephrochronology. In: Elias, S.A., Mock, C.J. (Eds.), The Encyclopaedia of Quaternary Science, second ed., vol. 4. Elsevier, London, pp. 277-304.

Barker, S.J., Wilson, C.J., Allan, A.S. and Schipper, C.I., 2015. Fine-scale temporal recovery, reconstruction and evolution of a post-supereruption magmatic system. *Contributions to Mineralogy and Petrology*, *170*(1), pp.1-40.

Barker, S.J., Wilson, C.J.N., Morgans, D.J. and Rowland, J.V., 2016. Rapid priming, accumulation, and recharge of magma driving recent eruptions at a hyperactive caldera volcano. Geology, 44, 323-326.

Barker, S.J., Van Eaton, A.R., Mastin, L.G., Wilson, C.J.N., Thompson, M.A., Wilson, T.M., Davis, C. and Renwick, J.A., 2019. Modeling ash dispersal from future eruptions of Taupo supervolcano. Geochemistry, Geophysics, Geosystems, 20(7), pp.3375-3401.

Barker, S.J., Wilson, C.J.N., Illsley-Kemp, F., Leonard, G.S., Mestel, E.R.H., Mauriohooho, K. and Charlier, B.L.A., 2021. Taupō: an overview of New Zealand's supervolcano. New Zealand Journal of Geology and Geophysics (in press) 10.1080/00288306.2020.1792515

Barrell, D.J.A., Almond, P.C., Vandergoes, M.J., Lowe, D.J., Newnham, R.M. and NZ-INTIMATE members, 2013. A composite pollen-based stratotype for inter-regional evaluation of climatic events in New Zealand over the past 30,000 years (NZ-INTIMATE project). Quaternary Science Reviews, 74, 4-20.

Beu, A.G. and Edwards, A.R., 1984. New Zealand Pleistocene and late Pliocene glacio-eustatic cycles. Palaeogeography, Palaeoclimatology, Palaeoecology, 46(1-3), pp.119-142.

Black, T.M., Shane, P.A., Westgate, J.A. and Froggatt, P.C., 1996. Chronological and palaeomagnetic constraints on widespread welded ignimbrites of the Taupo volcanic zone, New Zealand. Bulletin of Volcanology, 58(2-3), pp.226-238.

Bland, K.J., Kamp, P.J. and Nelson, C.S., 2007. Systematic lithostratigraphy of the Neogene succession exposed in central parts of Hawke's Bay Basin, eastern North Island, New Zealand. Ministry of Economic Development New Zealand Unpublished Petroleum Report PR3724, pp.259.

Bolton, M.S., Jensen, B.J., Wallace, K., Praet, N., Fortin, D., Kaufman, D. and De Batist, M., 2020. Machine learning classifiers for attributing tephra to source volcanoes: an evaluation of methods for Alaska tephras. Journal of Quaternary Science, 35(1-2), pp.81-92.

Briggs, R.M., Houghton, B.F., McWilliams, M. and Wilson, C.J.N., 2005. $^{40}Ar/^{39}Ar$ ages of silicic volcanic rocks in the TaurangaKaimai area, New Zealand: dating the transition between volcanism in the Coromandel Arc and the Taupo Volcanic Zone. New Zealand Journal of Geology and Geophysics, 48(3), pp.459-469.

Briggs, R.M., Lowe, D.J., Esler, W.R., Smith, R.T., Henry, M.A.C., Wehrmann, H. and Manning, D.A., 2006. Geology of the Maketu area, Bay of Plenty, North Island, New Zealand. Sheet V14 1:50000. Department of Earth and Ocean Sciences, University of Waikato, Occasional Report 26. 43 pp + Map

Buck, M.D., Briggs, R.M. and Nelson, C.S., 1981. Pyroclastic deposits and volcanic history of Mayor Island. New Zealand Journal of Geology and Geophysics, 24(4), pp.449-467.

Bussell, M.R., 1986. Palynological evidence for upper Putikian (middle Pleistocene) interglacial and glacial climates at Rangitawa Stream, south Wanganui Basin, New Zealand. New Zealand journal of geology and geophysics, 29(4), pp.471-479.

Bussell, M.R. and Pillans, B., 1997. Vegetational and climatic history during oxygen isotope stage 7 and early stage 6, Taranaki, New Zealand. Journal of the Royal Society of New Zealand, 27(4), pp.419-438.

035

Carter, R.M. and Naish, T.R., 1998. A review of Wanganui Basin, New Zealand: global reference section for shallow marine, Plio–Pleistocene (2.5–0 Ma) cyclostratigraphy. Sedimentary Geology, 122(1-4), pp.37-52.

040 Carter, L., Alloway, B., Shane, P. and Westgate, J., 2004. Deep-ocean record of major late Cenozoic rhyolitic eruptions from New Zealand. New Zealand Journal of Geology and Geophysics, 47(3), pp.481-500.

Carter, L., Shane, P., Alloway, B., Hall, I.R., Harris, S.E. and Westgate, J.A., 2003. Demise of one
045 volcanic zone and birth of another—a 12 my marine record of major rhyolitic eruptions from New Zealand. Geology, 31(6), pp.493-496.

Carter, L., Nelson, C.S., Neil, H.L. and Froggatt, P.C., 1995. Correlation, dispersal, and preservation of the Kawakawa Tephra and other late Quaternary tephra layers in the Southwest Pacific Ocean. New
050 Zealand Journal of Geology and Geophysics, 38(1), pp.29-46.

Carter, R.M., Abbott, S.T. and Naish, T.R., 1999. Plio-Pleistocene cyclothems from Wanganui Basin, New Zealand: type locality for an astrochronologic time-scale, or template for recognizing ancient glacio-eustacy?. Philosophical Transactions of the Royal Society of London. Series A: Mathematical,
055 Physical and Engineering Sciences, 357(1757), pp.1861-1872.

Charlier, B. L. A. and Wilson, C. J. N., 2010. Chronology and evolution of caldera-forming and post caldera magma systems at Okataina Volcano, New Zealand from zircon U–Th model-age spectra. Journal of Petrology, 51(5), pp.1121-1141.
060

Cole, J.W., Deering, C.D., Nairn, Burt, R.M., Sewell, S., Shane, P.A.R. and Matthews, N.E., 2014. Okataina Volcanic Centre, Taupo Volcanic Zone, New Zealand: A review of volcanism and synchronous pluton development in an active, dominantly silicic caldera system. Earth Science Reviews, 128, pp.1-17.
065

Cooper, G.F., Wilson, C.J.N., Millet, M-A, Baker, J.A. and Smith, E.G.C., 2012. Systematic tapping of independent magma chambers during the 1 Ma Kidnappers supereruption. Earth and Planetary Science Letters, 313, pp.23-33.

070 Curran, J., 2018. Hotelling: Hotelling's T^2 Test and Variants. R package version 1.0-5. https://CRAN.R-project.org/package=Hotelling

Danišík, M., Shane, P., Schmitt, A.K., Hogg, A., Santos, G.M., Storm, S., Evans, N.J., Fifield, L.K. and Lindsay, J.M., 2012. Re-anchoring the late Pleistocene tephrochronology of New Zealand based on concordant radiocarbon ages and combined $^{238}U/^{230}Th$ disequilibrium and (U–Th)/He zircon ages. Earth and Planetary Science Letters, 349, pp.240-250.

Danišík, M., Lowe, D.J., Schmitt, A.K., Friedrichs, B., Hogg, A.G., Evans, N.J. 2020. Sub-millennial eruptive recurrence in the silicic Mangaone Subgroup tephra sequence, New Zealand, from Bayesian modelling of zircon double-dating and radiocarbon ages. Quaternary Science Reviews, 246, article 106517.

Denton, J.S. and Pearce, N.J., 2008. Comment on "A synchronized dating of three Greenland ice cores throughout the Holocene" by BM Vinther et al.: No Minoan tephra in the 1642 BC layer of the GRIP ice core. Journal of Geophysical Research, 113(D4), p.D04303.

Dugmore, A.J., Larsen, G. and Newton, A.J., 2004. Tephrochronology and its application to late Quaternary environmental reconstruction, with special reference to the North Atlantic islands. In: Buck, C.E., Millard A.R. (Eds), Tools for Constructing Chronologies: Cross Disciplinary Boundaries. Lecture Notes in Statistics, vol. 177. Springer, London, pp. 173-188.

Erdman, C.F. and Kelsey, H.M., 1992. Pliocene and Pleistocene stratigraphy and tectonics, Ohara Depression and Wakarara Range, North Island, New Zealand. New Zealand Journal of Geology and Geophysics, 35(2), pp.177-192.

Ewart, A., 1968. The Petrography of the Central North Island Rhyolitic Lavas: Part 2—Regional Petrography Including Notes on Associated Ash-Flow Pumice Deposits. New Zealand Journal of Geology and Geophysics, 11(2), pp.478-545.

Flude, S. and Storey, M., 2016. 40Ar/39Ar age of the Rotoiti Breccia and Rotoehu Ash, Okataina Volcanic Complex, New Zealand, and identification of heterogeneously distributed excess 40Ar in supercooled crystals. Quaternary Geochronology, 33, pp.13-23.

Froggatt, P.C., 1983. Toward a comprehensive Upper Quaternary tephra and ignimbrite stratigraphy in New Zealand using electron microprobe analysis of glass shards. Quaternary research, 19(2), pp.188-200.

Froggatt, P.C., 1992. Standardization of the chemical analysis of tephra deposits. Report of the ICCT working group. Quaternary International, 13-14, pp.93-96.

Froggatt, P.C. and Lowe, D.J., 1990. A review of late Quaternary silicic and some other tephra formations from New Zealand: their stratigraphy, nomenclature, distribution, volume, and age. New Zealand Journal of Geology and Geophysics, 33(1), pp.89-109.

115 Froggatt, P.C. and Rogers, G.M., 1990. Tephrostratigraphy of high-altitude peat bogs along the axial ranges, North Island, New Zealand, New Zealand Journal of Geology and Geophysics, 33, pp.111-124.

Gehrels, M.J., Lowe, D.J., Hazell, Z.J. and Newnham, R.M., 2006. A continuous 5300-yr Holocene cryptotephrostratigraphic record from northern New Zealand and implications for tephrochronology and
120 volcanic hazard assessment. The Holocene, 16(2), pp.173-187.

Grant, G.R., Sefton, J.P., Patterson, M.O., Naish, T.R., Dunbar, G.B., Hayward, B.W., Morgans, H.E.G., Alloway, B.V., Seward, D., Tapia, C.A. and Prebble, J.G., 2018. Mid-to late Pliocene (3.3–2.6 Ma) global sea-level fluctuations recorded on a continental shelf transect, Whanganui Basin, New
125 Zealand. Quaternary Science Reviews, 201, pp.241-260.

Grant, G.R., Naish, T.R., Dunbar, G.B., Stocchi, P., Kominz, M.A., Kamp, P.J., Tapia, C.A., McKay, R.M., Levy, R.H. and Patterson, M.O., 2019. The amplitude and origin of sea-level variability during the Pliocene epoch. Nature, 574(7777), pp.237-241.
130
Gravley, D.M., Wilson, C.J.N., Leonard, G.S. and Cole, J.W., 2007. Double trouble: Paired ignimbrite eruptions and collateral subsidence in the Taupo Volcanic Zone, New Zealand. Geological Society of America Bulletin, 119(1-2), pp.18-30.
1
135
Gravely, D.M., Wilson, C.J.N., Rosenberg, M.D. and Leonard, G.S., 2006. The nature and age of Ohakuri Formation and Ohakuri Group rocks in surface exposures and geothermal drillhole sequences in the central Taupo Volcanic Zone, New Zealand. New Zealand Journal of Geology and Geophysics, 49:3, pp.305-308.
140
Hogg, A.G. and McCraw, J.D., 1983. Late Quaternary tephras of Coromandel Peninsula, North Island, New Zealand: a mixed peralkaline and calcalkaline tephra sequence. New Zealand Journal of Geology and Geophysics, 26(2), pp.163-187.

145 Hogg, A.G., Higham, T.F.G., Lowe, D.J., Palmer, J., Reimer, P. and Newnham, R.M., 2003. A wiggle-match date for Polynesian settlement of New Zealand. Antiquity, 77, pp.116-125.

Hogg, A.G., Lowe, D.J., Palmer, J.G., Boswijk, G. and Bronk Ramsey, C.J., 2012. Revised calendar date for the Taupo eruption derived by ^{14}C wiggle-matching using a New Zealand kauri ^{14}C calibration
150 data set. The Holocene, 22, 439-449.

Hogg, A.G., Wilson, C.J.N., Lowe, D.J., Turney, C.S.M., White, P., Lorrey, A.M., Manning, S.W., Palmer, J.G., Bury, S., Brown, J., Southon, J. and Petchey, F., 2019. Wiggle-match radiocarbon dating of the Taupo eruption. Nature Communications, 10, 4669.
155

Holt, K.A., Lowe, D.J., Hogg, A.G. and Wallace, R.C., 2011. Distal occurrence of mid-Holocene Whakatane Tephra on the Chatham Islands, New Zealand, and potential for cryptotephra studies. Quaternary International, 246, pp.344-351.

160 Holt, K., Wallace, R.C., Neall, V.E., Kohn, B.P. and Lowe, D.J., 2010. Quaternary tephra marker beds and their potential for palaeoenvironmental reconstruction on Chatham Islands east of New Zealand, southwest Pacific Ocean. Journal of Quaternary Science, 25, pp.1169-1178.

Hopkins, J.L. and Seward, D., 2019. Towards robust tephra correlations in early and pre-Quaternary
165 sediments: A case study from North Island, New Zealand. Quaternary Geochronology, 50, pp.91-108.

Hopkins, J.L., Wysoczanski, R.J., Orpin, A.R., Howarth, J.D., Strachan, L.J., Lunenburg, R., McKeown, M., Ganguly, A., Twort, E. and Camp, S., 2020. Deposition and preservation of tephra in marine sediments at the active Hikurangi subduction margin. Quaternary Science Reviews, 274,
170 doi.org,10.1016/j.quascirev.2020.106500.

Hopkins, J.L., Wilson, C.J., Millet, M.A., Leonard, G.S., Timm, C., McGee, L.E., Smith, I.E. and Smith, E.G., 2017. Multi-criteria correlation of tephra deposits to source centres applied in the Auckland Volcanic Field, New Zealand. Bulletin of Volcanology, 79(7), p.55.
175
Hopkins, J.L., Millet, M.A., Timm, C., Wilson, C.J., Leonard, G.S., Palin, J.M. and Neil, H., 2015. Tools and techniques for developing tephra stratigraphies in lake cores: a case study from the basaltic Auckland Volcanic Field, New Zealand. Quaternary Science Reviews, 123, pp.58-75.

180 Hopkins, J.L., Lowe, D.J., Horrocks, J.L., 2021. Tephrochronology in Aotearoa New Zealand. New Zealand Journal of Geology and Geophysics, 64 (2), pp. 153-200, doi:10.1080/00288306.2021.1908368

Houghton, B.F., Wilson, C.J.N., McWilliams, M.O., Lanphere, M.A., Weaver, S.D., Briggs, R.M. and Pringle, M.S., 1995. Chronology and dynamics of a large silicic magmatic system: central Taupo
185 Volcanic Zone, New Zealand. Geology, 23(1), pp.13-16.

Howorth, R. 1975. New formations of late Pleistocene tephras from the Okataina Volcanic Centre, New Zealand. New Zealand Journal of Geology and Geophysics, 18(5), pp.683-712.

190 Hunt, J.B., Fannin, N.G., Hill, P.G. and Peacock, J.D., 1995. The tephrochronology and radiocarbon dating of North Atlantic, Late-Quaternary sediments: an example from the St. Kilda Basin. Geological Society of London, Special Publications, 90(1), pp.227-248.

Iso, N., Okada, A., Ota, Y. and Yoshikawa, T., 1982. Fission-track ages of late Pleistocene tephra on the
195 Bay of Plenty coast, North Island, New Zealand. New Zealand Journal of Geology and Geophysics, 25(3), pp.295-303.

Jarosewich, E., Nelen, J.A. and Norberg, J.A., 1980. Reference samples for electron microprobe analysis. *Geostandards Newsletter*, *4*(1), pp.43-47.

Jochum, K.P., Stoll, B., Herwig, K., Willbold, M., Hofmann, A.W., Amini, M., Aarburg, S., Abouchami, W., Hellebrand, E., Mocek, B. and Raczek, I., 2006. MPI-DING reference glasses for in situ microanalysis: New reference values for element concentrations and isotope ratios. *Geochemistry, Geophysics, Geosystems*, *7*(2).

Jurado-Chichay, Z. and Walker, G. P. L., 2000. Stratigraphy and dispersal of the Mangaone Subgroup pyroclastic deposits, Okataina Volcanic Centre, New Zealand. Journal of Volcanology and Geothermal Research, 104(1-4), pp.319-380.

Kassambara, A., and Mundt, F., 2020. factoextra: Extract and Visualize the Results of Multivariate Data Analyses. R package version 1.0.7. https://CRAN.R-project.org/package=factoextra

Kilgour, G.N. and Smith, R.T. 2008. Stratigraphy, dynamics, and eruption impacts of the dual magma Rotorua eruptive episode, Okataina Volcanic Centre, New Zealand, New Zealand Journal of Geology and Geophysics 51, pp.367-378.

Klemetti, E. W., Deering, C. D., Cooper, K. M. and Roeske, S. M., 2011. Magmatic perturbations in the Okataina Volcanic Complex, New Zealand at thousand-year timescales recorded in single zircon crystals. Earth and Planetary Science Letters, 305(1-2), pp.185-194.

Knott, J.R., Sarna-Wojcicki, A.M., Montañez, I.P. and Wan, E., 2007. Differentiating the Bishop ash bed and related tephra layers by elemental-based similarity coefficients of volcanic glass shards using solution inductively coupled plasma-mass spectrometry (S-ICP-MS). Quaternary International, 166(1), pp.79-86.

Kobayashi, T., Nairn, I., Smith, V. and Shane, P., 2005. Proximal stratigraphy and event sequence of the c. 5600 cal. yr BP Whakatane rhyolite eruption episode from Haroharo volcano, Okataina Volcanic Centre, New Zealand. New Zealand Journal of Geology and Geophysics 48, pp.471-490.

Kuehn, S.C., Froese, D.G., Carrara, P.E., Foit, F.F., Pearce, N.J. and Rotheisler, P., 2009. The latest Pleistocene Glacier Peak tephra set revisited and revised: Major-and trace-element characterization, distribution, and a new chronology in western North America. Quaternary Research, 71, pp.201-216.

Kuehn, S.C., Froese, D.G., Shane, P.A.R. and INTAV Intercomparison Participants, 2011. The INTAV intercomparison of electron-beam microanalysis of glass by tephrochronology laboratories: results and recommendations. Quaternary International 246, pp.19-47.

Kurbatov, A., Dunbar, N.W., Iverson, N.A., Gerbi, C.C., Yates, M.G., Kalteyer, D. and McIntosh, W.C., 2014, December. Antarctic Tephra Database (AntT). In AGU Fall Meeting Abstracts.
240   (http://www.tephrochronology.org/AntT/)

Le Maitre, R.W., 1984. A proposal by the IUGS Subcommission on the Systematics of Igneous Rocks for a chemical classification of volcanic rocks based on the total alkali silica (TAS) diagram: (on behalf of the IUGS Subcommission on the Systematics of Igneous Rocks). Australian Journal of Earth
245   Sciences, 31(2), pp.243-255.

Leahy, K., 1997. Discrimination of reworked pyroclastics from primary tephra-fall tuffs: a case study using kimberlites of Fort a la Corne, Saskatchewan, Canada. Bulletin of Volcanology 59, pp.65-71.

250   Lowe, D.J., 2019. Using soil stratigraphy and tephrochronology to understand the origin, age, and classification of a unique Late Quaternary tephra-derived Ultisol in Aotearoa New Zealand. Quaternary, 2(1), article 9. https://doi.org/10.3390/quat2010009

Lowe, D.J., 2014. Marine tephrochronology: a personal perspective. Geological Society, London,
255   Special Publications, 398(1), pp.7-19.

Lowe, D.J., 2011. Tephrochronology and its application: a review. Quaternary Geochronology, 6(2), pp.107-153.

260   Lowe, D.J., 1988. Late Quaternary volcanism in New Zealand: towards an integrated record using distal airfall tephras in lakes and bogs. Journal of Quaternary Science, 3, pp.111–120.

Lowe, D.J. and Newnham, R.M., 2004. Role of tephra in dating Polynesian settlement and impact, New Zealand. Past Global Changes, 12 (3), pp.5-7.
265

Lowe, D.J., Rees, A.B.H., Newnham, R.M., Hazell, Z.J., Gehrels, M.J., Charman, D.J. and Amesbury, M.J., 2019. Isochron-informed Bayesian age modelling for tephras and cryototephras, and application to mid-Holocene Tuhua tephra, New Zealand. 20th INQUA Congress, Dublin, 25-31 July 2019 (abstract P-4604, 1 p.).
270

Lowe, D.J., Pearce, N.J.G., Jorgensen, M.A., Kuehn, S.C., Tryon, C.A., and Hayward, C.L., 2017. Correlating tephras and cryptotephras using glass compositional analyses and numerical and statistical methods: review and evaluation. Quaternary Science Reviews, 175, pp.1-44

275   Lowe, D.J., Blaauw, M., Hogg, A.G. and Newnham, R.M., 2013. Ages of 24 widespread tephras erupted since 30,000 years ago in New Zealand, with re-evaluation of the timing and palaeoclimatic implications of the Lateglacial cool episode recorded at Kaipo bog. Quaternary Science Reviews, 74, pp.170-194.

280   Lowe, D.J., Shane, P.A., Alloway, B.V. and Newnham, R.M., 2008. Fingerprints and age models for widespread New Zealand tephra marker beds erupted since 30,000 years ago: a framework for NZ-INTIMATE. Quaternary Science Reviews, 27(1-2), pp.95-126.

Lowe, D.J., Tippett, J.M., Kamp, P.J., Liddell, I.J., Briggs, R.M. and Horrocks, J.L., 2001. Ages on
285   weathered Plio-Pleistocene tephra sequences, western North Island, New Zealand. Les Dossiers de l'Archéo-Logis, 1, pp.45-60.

Lowe, D.J., Newnham, R.M. and Ward, C.M., 1999. Stratigraphy and chronology of a 15 ka sequence of multi-sourced silicic tephras in a montane peat bog, eastern North Island, New Zealand. New
290   Zealand Journal of Geology and Geophysics, 42(4), pp.565-579.

Manning, D.A., 1996. Middle-late Pleistocene tephrostratigraphy of the eastern Bay of Plenty, New Zealand. Quaternary International, 34, pp.3-12.

295   Mahony, S.H., Barnard, N.H., Sparks, R.S.J. and Rougier, J.C., 2020. VOLCORE, a global database of visible tephra layers sampled by ocean drilling. Scientific Data, 7(1), pp.1-17.

McDonough, W.F. and Sun, S.S., 1995. The composition of the Earth. Chemical geology, 120(3-4), pp.223-253.
300
Milner, D.M., Cole, J.W. and Wood, C.P., 2003. Mamaku Ignimbrite: a caldera-forming ignimbrite erupted from a compositionally zoned magma chamber in Taupo Volcanic Zone, New Zealand. Journal of Volcanology and Geothermal Research, 122(3-4), pp.243-264.

305   Molloy, C.M., 2008. Tephrostratigraphy of the Auckland Maar Craters. MSc thesis, University of Auckland, Auckland, New Zealand.

Molloy, C., Shane, P. and Augustinus, P., 2009. Eruption recurrence rates in a basaltic volcanic field based on tephra layers in maar sediments: implications for hazards in the Auckland volcanic
310   field. Geological Society of America Bulletin, 121(11-12), pp.1666-1677.

Mortimer, N. and Scott, J.M., 2020. Volcanoes of Zealandia and the Southwest Pacific. New Zealand Journal of Geology and Geophysics, 63(4), pp.371-377.

315   Nairn, I.A., 2002. Geology of the Okataina Volcanic Centre, scale 1: 50 000. Institute of Geological and Nuclear Sciences geological map 25. 1 sheet+ 156 p. Institute of Geological and Nuclear Sciences Ltd.

Nairn, I.A., 1992. The Te Rere and Okareka eruptive episodes — Okataina Volcanic Centre, Taupo Volcanic Zone, New Zealand. New Zealand Journal of Geology and Geophysics, 35, pp.93-108.
320

Nairn, I.A. and Kohn, B.P., 1973. Relation of the Earthquake Flat Breccia to the Rotoiti Breccia, central North Island, New Zealand. New Zealand Journal of Geology and Geophysics, 16(2), pp.269-279.

Nairn, I.A., Shane, P.R., Cole, J.W., Leonard, G.J., Self, S. and Pearson, N., 2004. Rhyolite magma processes of the∼ AD 1315 Kaharoa eruption episode, Tarawera volcano, New Zealand. Journal of Volcanology and Geothermal Research, 131(3-4), pp.265-294.

Naish, T., and Kamp, P.J., 1997. Foraminiferal depth palaeoecology of Late Pliocene shelf sequences and systems tracts, Wanganui Basin, New Zealand. Sedimentary Geology, 110(3-4), pp.237-255.

Naish, T., and Kamp, P.J., 1995. Pliocene-Pleistocene marine cyclothems, Wanganui Basin, New Zealand: A lithostratigraphic framework. New Zealand Journal of Geology and Geophysics, 38(2), pp.223-243.

Naish, T.R., Field, B.D., Zhu, H., Melhuish, A., Carter, R.M., Abbott, S.T., Edwards, S., Alloway, B.V., Wilson, G.S., Niessen, F. and Barker, A., 2005. Integrated outcrop, drill core, borehole and seismic stratigraphic architecture of a cyclothemic, shallow-marine depositional system, Wanganui Basin, New Zealand. Journal of the Royal Society of New Zealand, 35(1-2), pp.91-122.

Naish, T., Kamp, P.J., Alloway, B.V., Pillans, B., Wilson, G.S. and Westgate, J.A., 1996. Integrated tephrochronology and magnetostratigraphy for cyclothemic marine strata, Whanganui Basin: implications for the Pliocene-Pleistocene boundary in New Zealand. Quaternary International, 34, pp.29-48.

Nelson, C.S., Froggatt, P.C. and Gosson, G.J., 1985. Nature, chemistry, and origin of late Cenozoic megascopic tephras in Leg 90 cores from the southwest Pacific. In: Kennett, J.P. & Von Der Borch, C. C. (eds) Proceedings of the Ocean Drilling Program, Initial Reports, 90. Ocean Drilling Program, Texas A & M University, College Station, TX, pp.1160–1173.

Newnham, R.M., Hazell, Z.J., Charman, D.J., Lowe, D.J., Rees, A.B.H., Amesbury, M.J., Roland, T.P., Gehrels, M.J., van den Bos, V., and Jara, I.A. 2019. Peat humification records from Restionaceae bogs in northern New Zealand as potential indicators of Holocene precipitation, seasonality, and ENSO. Quaternary Science Reviews, 218, pp.378-394.

Newnham, R.M., Vandergoes, M.J., Garnett, M.H., Lowe, D.J., Prior, C. and Almond, P.C., 2007. Test of AMS ^{14}C dating of pollen concentrates using tephrochronology. Journal of Quaternary Science, 22(1), pp.37-51.

Newnham, R.M., Lowe, D.J., Green, J.D., Turner, G.M., Harper, M.A., McGlone, M.S., Stout, S.L., Horie, S. and Froggatt, P.C. 2004. A discontinuous ca. 80 ka record of Late Quaternary environmental change from Lake Omapere, Northland, New Zealand. Palaeogeography, Palaeoclimatology, Palaeoecology, 207, pp.165-198.

Newnham, R.M., Eden, D.N., Lowe, D.J. and Hendy, C.H., 2003. Rerewhakaaitu Tephra, a land–sea
365 marker for the Last Termination in New Zealand, with implications for global climate
change. Quaternary Science Reviews, 22(2-4), pp.289-308.

Newnham, R.M., Lowe, D.J., McGlone, M.S., Wilmshurst, J.M. and Higham, T.F.G., 1998. The
Kaharoa Tephra as a critical datum for earliest human impact in northern New Zealand. Journal of
370 Archaeological Science, 25(6), pp.533-544.

Newnham, R.M., De Lange, P.J. and Lowe, D.J., 1995. Holocene vegetation, climate and history of a
raised bog complex, northern New Zealand based on palynology, plant macrofossils and
tephrochronology. The Holocene, 5(3), pp.267-282.
375
Newton, A., 1996. Tephrabase. A tephrochronological database. Quaternary Newsletter, pp.8-13.
(https://www.tephrabase.org/)

Nicol, A., VanDissen, R., Vella, P., Alloway, B. and Melhuish, A., 2002. Growth of contractional
380 structures during the last 10 my at the southern end of the emergent Hikurangi forearc basin, New
Zealand. New Zealand Journal of Geology and Geophysics, 45(3), pp.365-385.

Oksanen, J., Guillaume Blanchet, F., Friendly, M., Kindt, R., Legendre, P., McGlinn, D., Minchin, P.R.,
O'Hara, R.B., Simpson, G.L., Solymos, P., Henry, M., Stevens, H., Szoecs, E., Wagner, H., 2019.
385 vegan: Community Ecology Package. R package version 2.5-6. https://CRAN.R
project.org/package=vegan

Orpin, A.R., Carter, L., Page, M.J., Cochrn, U.A., Trustrum, N.A., Gomez, B., Palmer, A.S.,
Mildenhall, D.C., Rogers, K.M., Brackly, H.L. and Northcote, L., 2010. Holocene sedimentary record
390 from Lake Tutira: a template for upland watershed erosion proximal to the Waipaoa Sedimentary
System, northeastern New Zealand. Marine Geology, 270, pp.11–29.

Pain, C.F., 1975. Some tephra deposits in the south-west Waikato area, North Island, New Zealand.
New Zealand Journal of Geology and Geophysics, 18, pp.541-550.
395
Paton, C., Hellstrom, J., Paul, B., Woodhead, J. and Hergt, J., 2011. Iolite: Freeware for the
visualisation and processing of mass spectrometric data. Journal of Analytical Atomic
Spectrometry, 26(12), pp.2508-2518.

400 Pearce, N.J., 2014. Towards a protocol for the trace element analysis of glass from rhyolitic shards in
tephra deposits by laser ablation ICP-MS. Journal of Quaternary Science, 29(7), pp.627-640.

Pearce, N.J., Perkins, W.T., Westgate, J.A. and Wade, S.C., 2011. Trace-element microanalysis by LA-ICP-MS: the quest for comprehensive chemical characterisation of single, sub-10 μm volcanic glass shards. Quaternary International, *246*(1-2), pp.57-81.

Pearce, N.J., Alloway, B.V. and Westgate, J.A., 2008. Mid-Pleistocene silicic tephra beds in the Auckland region, New Zealand: their correlation and origins based on the trace element analyses of single glass shards. Quaternary International, 178(1), pp.16-43.

Pearce, N.J., Denton, J.S., Perkins, W.T., Westgate, J.A. and Alloway, B.V., 2007. Correlation and characterisation of individual glass shards from tephra deposits using trace element laser ablation ICP-MS analyses: current status and future potential. Journal of Quaternary Science, 22(7), pp.721-736.

Pearce, N.J., Westgate, J.A., Perkins, W.T. and Preece, S.J., 2004. The application of ICP-MS methods to tephrochronological problems. Applied Geochemistry, 19(3), pp.289-322.

Pearce, N.J., Eastwood, W.J., Westgate, J.A. and Perkins, W.T., 2002. Trace-element composition of single glass shards in distal Minoan tephra from SW Turkey. Journal of the Geological Society, 159(5), pp.545-556.

Pearce, N.J., Westgate, J.A. and Perkins, W.T., 1996. Developments in the analysis of volcanic glass shards by laser ablation ICP-MS: quantitative and single internal standard-multielement methods. Quaternary International, 34, pp.213-227.

Pecher, I.A., Barnes, P.M., LeVay, L.J. and the Expedition 372 Scientists, 2018. Expedition 372 Preliminary Report: Creeping Gas Hydrate Slides and Hikurangi LWD. International Ocean Discovery Program. https://doi.org/10.14379/iodp.pr.372.2018

Peti, L., Gadd, P.S., Hopkins, J.L. and Augustinus, P.C., 2020. Itrax μ-XRF core scanning for rapid tephrostratigraphic analysis: a case study from the Auckland Volcanic Field maar lakes. Journal of Quaternary Science, 35(1-2), pp.54-65.

Peti, L., Hopkins, J.L., Augustinus, P. 2021. Revised tephrochronology for key tephras in the 130-ka Ōrākei Basin maar core, Auckland Volcanic Field, New Zealand: implications for the timing of climatic changes, New Zealand. New Zealand Journal of Geology and Geophysics (in press) https://doi.org/10.1080/00288306.2020.1867200

Pillans, B., 2017. Quaternary stratigraphy of Whanganui Basin—a globally significant archive. In Landscape and quaternary environmental change in New Zealand (pp. 141-170). Atlantis Press, Paris.

Pillans, B., 1994. Direct marine-terrestrial correlations, Wanganui Basin, New Zealand: the last 1 million years. Quaternary science reviews, 13(3), pp.189-200.

445

Pillans, B., Alloway, B., Naish, T., Westgate, J., Abbott, S. and Palmer, A., 2005. Silicic tephras in Pleistocene shallow-marine sediments of Wanganui Basin, New Zealand. Journal of the Royal Society of New Zealand, 35(1-2), pp.43-90.

450 Pillans, B.J., Roberts, A.P., Wilson, G.S., Abbott, S.T. and Alloway, B.V., 1994. Magnetostratigraphic, lithostratigraphic and tephrostratigraphic constraints on Lower and Middle Pleistocene sea-level changes, Wanganui Basin, New Zealand. Earth and Planetary Science Letters, 121(1-2), pp.81-98.

Pittari, A., Prentice, M.L., McLeod, O.E., Yousefzadeh, E., Kamp, P.J.J., Danišík, M., Vincent, K.A., 2021. Inception of the modern North Island (New Zealand) volcanic setting: spatio-temporal patterns of 455 volcanism between 3.0 and 0.9 Ma. New Zealand Journal of Geology and Geophysics 64 (2) in press https://doi.org/10.1080/00288306.2021.1915343

Portnyagin, M.V., Ponomareva, V.V., Zelenin, E.A., Bazanova, L.I., Pevzner, M.M., Plechova, A.A., Rogozin, A.N. and Garbe-Schönberg, D., 2020. TephraKam: geochemical database of glass compositions in tephra and welded tuffs from the Kamchatka volcanic arc (northwestern Pacific). Earth 460 System Science Data, 12(1), pp.469-486.

Preece, S.J., Westgate, J.A., Froese, D.G., Pearce, N.J.G. and Perkins, W.T., 2011. A catalogue of late Cenozoic tephra beds in the Klondike goldfields, Yukon. Canadian Journal of Earth Sciences, 48, pp.1386-1418.
465

R Core Team (2019). R: A language and environment for statistical computing. R Foundation for Statistical Computing, Vienna, Austria. URL https://www.R-project.org/.

Rees, C., Palmer, J. and Palmer, A., 2018. Plio-Pleistocene geology of the lower Pohangina valley, New 470 Zealand. New Zealand Journal of Geology and Geophysics, 61(1), pp.44-63.

Rees, C., Palmer, A. and Palmer, J., 2019. Quaternary sedimentology and tephrostratigraphy of the lower Pohangina Valley, New Zealand. New Zealand Journal of Geology and Geophysics, 62(2), pp.171-194.
475

Rees, C., Palmer, J. and Palmer, A., 2020. Tephrostratigraphic constraints on sedimentation and tectonism in the Whanganui Basin, New Zealand. New Zealand Journal of Geology and Geophysics, 63(2), pp. 262-280.

480 Rosenberg, M.D., Wilson, C.J.N., Bignall, G., Ireland, T.R., Sepulveda, F. and Charlier, B.L.A., 2020. Structure and evolution of the Wairakei–Tauhara geothermal system (Taupo Volcanic Zone, New Zealand) revisited with a new zircon geochronology. Journal of Volcanology and Geothermal Research, 390, 106705.

485 Rubin, A. E., Cooper, K. M., Leever, M., Wimpenny, J., Deering, C., Rooney, T., Gravley, D. and Yin, Q-Z., 2016: Changes in magma storage conditions following caldera collapse at Okataina Volcanic Center, New Zealand. Contributions to Mineralogy and Petrology, 171, pp.1-18.

Saffer, D.M., Wallace, L.M., Petronotis, K. and the Expedition 375 Scientists, 2018. Expedition 375
490 Preliminary Report: Hikurangi Subduction Margin Coring and Observatories. International Ocean Discovery Program. https://doi.org/10.14379/iodp.pr.375.2018

Sahetapy-Engel, S., Self, S., Carey, R.J. and Nairn, I.A., 2014. Deposition and generation of multiple widespread fall units from the *c*. AD 1314 Kaharoa rhyolitic eruption, Tarawera, New Zealand. Bulletin
495 of Volcanology 76, article 836: DOI 10.1007/s00445-014-0836-4.

Sandiford, A., Horrocks, M., Newnham, R., Ogden, J. and Alloway, B., 2002. Environmental change during the last glacial maximum (c. 25 000-c. 16 500 years BP) at Mt Richmond, Auckland Isthmus, New Zealand. Journal of the Royal Society of New Zealand, 32(1), pp.155-167.
500
Sarna-Wojcicki, A.M., 2000. Tephrochronology. In: Noller, J.S., Sowers, J.M., Lettis, W.R., (Eds.), Quaternary Geochronology: Methods and Applications. AGU Reference Shelf. Vol. 4. American Geophysical Union Washington, DC, pp. 357-377.

505 Saul, G., Naish, T.R., Abbott, S.T. and Carter, R.M., 1999. Sedimentary cyclicity in the marine Pliocene-Pleistocene of the Wanganui basin (New Zealand): Sequence stratigraphic motifs characteristic of the past 2.5 my. Geological Society of America Bulletin, 111(4), pp.524-537.

Saunders, K.E., Baker, J.A. and Wysoczanski, R.J., 2010. Microanalysis of large volume silicic magma
510 in continental and oceanic arcs: Melt inclusions in Taupo Volcanic Zone and Kermadec Arc rocks, South West Pacific. Journal of Volcanology and Geothermal Research, 190(1-2), pp.203-218.

Schneider, J.L., Le Ruyet, A., Chanier, F., Buret, C., Ferrière, J., Proust, J.N. and Rosseel, J.B., 2001. Primary or secondary distal volcaniclastic turbidites: how to make the distinction? An example from the
515 Miocene of New Zealand (Mahia Peninsula, North Island). Sedimentary Geology, 145(1-2), pp.1-22.

Seward, D., 1976. Tephrostratigraphy of the marine sediments in the Wanganui Basin, New Zealand. New Zealand journal of Geology and Geophysics, 19(1), pp.9-20.

520 Shane, P.A.R., 2000. Tephrochronology: a New Zealand case study. Earth-Science Reviews 49, pp.223-259.

Shane, P.A.R., 1998. Correlation of rhyolitic pyroclastic eruptive units from the Taupo volcanic zone by Fe–Ti oxide compositional data. Bulletin of Volcanology, 60(3), pp.224-238.
525

Shane, P.A.R., 1994. A widespread, early Pleistocene tephra (Potaka tephra, 1 Ma) in New Zealand: character, distribution, and implications. New Zealand Journal of Geology and Geophysics, 37, pp.25-35.

530   Shane, P.A.R. and Froggatt, P.C., 1991. Glass chemistry, paleomagnetism, and correlation of middle Pleistocene tuffs in southern North Island, New Zealand, and Western Pacific. New Zealand journal of geology and geophysics, 34(2), pp.203-211.

Shane, P.A.R. and Hoverd, J., 2002. Distal record of multi-sourced tephra in Onepoto Basin, Auckland,
535   New Zealand: implications for volcanic chronology, frequency and hazards. Bulletin of Volcanology, 64(7), pp.441-454.

Shane, P., Gehrels, M., Zawalna-Geer, A., Augustinus, P., Lindsay, J. and Chaillou, I., 2013. Longevity of a small shield volcano revealed by crypto-tephra studies (Rangitoto volcano, New Zealand): change
540   in eruptive behavior of a basaltic field. Journal of Volcanology and Geothermal Research, 257, pp.174-183.

Shane, P., Nairn, I.A., Martin, S.B. and Smith, V.C., 2008. Compositional heterogeneity in tephra deposits resulting from the eruption of multiple magma bodies: implications for
545   tephrochronology. Quaternary International, 178(1), pp.44-53.

Shane, P.A.R., Sikes, E.L. and Guilderson, T.P., 2006. Tephra beds in deep-sea cores off northern New Zealand: implications for the history of Taupo volcanic zone, Mayor Island and White Island volcanoes. Journal of Volcanology and Geothermal Research, 154, pp.276-290.
550
Shane, P.A.R., Smith, V.C. and Nairn, I.A., 2005. High temperature rhyodacites of the 36 ka Hauparu pyroclastic eruption, Okataina Volcanic Centre, New Zealand: change in a silicic magmatic system following caldera collapse. Journal of Volcanology and Geothermal Research,147, pp.357-376.

555   Shane, P.A.R., Smith, V.C., Lowe, D.J. and Nairn, I.A., 2003a. Re-identification of c. 15 700 cal yr BP tephra bed at Kaipo Bog, eastern North Island: implications for dispersal of Rotorua and Puketarata tephra beds. New Zealand Journal of Geology and Geophysics 46, 591-596.

Shane, P.A.R., Smith, V.C. and Nairn, I.A., 2003b. Biotite composition as a tool for the identification of
560   Quaternary tephra beds. Quaternary Research 59, pp.262-270.

Shane, P., Lian, O.B., Augustinus, P., Chisari, R. and Heijnis, H., 2002. Tephrostratigraphy and geochronology of a ca. 120 ka terrestrial record at Lake Poukawa, North Island, New Zealand. Global and Planetary Change, 33(3-4), pp.221-242.
565

Shane, P.A.R, Black, T.M., Alloway, B.V. and Westgate, J.A., 1996. Early to middle Pleistocene tephrochronology of North Island, New Zealand: Implications for volcanism, tectonism, and paleoenvironments. Geological Society of America Bulletin, 108(8), pp.915-925.

570   Shane, P.A.R., Froggatt, P., Black, T. and Westgate, J., 1995. Chronology of Pliocene and Quaternary bioevents and climatic events from fission-track ages on tephra beds, Wairarapa, New Zealand. Earth and Planetary Science Letters, 130(1-4), pp.141-154.

Shane, P.A.R., Black, T. J. and Westgate, J.A., 1994. Isothermal plateau fission-track age for a
575   paleomagnetic excursion in the Mamaku Ignimbrite, New Zealand, and implications for Late Quaternary stratigraphy. Geophysical Research Letters, 21, pp.1695-1698.

Smith, V.C., Shane, P. and Smith, I.E.M., 2002. Tephrostratigraphy and geochemical fingerprinting of the Mangaone Subgroup tephra beds, Okataina volcanic centre, New Zealand. New Zealand Journal of
580   Geology and Geophysics, 45(2), pp.207-219.

Smith, V.C., Shane, P. and Nairn, I.A., 2004. Reactivation of a rhyolite magma body by new rhyolitic intrusion before the 15.8 ka Rotorua eruptive episode: implications for magma storage in the Okataina Volcanic Centre, New Zealand. Journal of the Geological Society of London, 161, pp.757-772.
585

Smith, V. C., Shane, P. and Nairn, I. A., 2005. Trends in rhyolite geochemistry, mineralogy, and magma storage during the last 50 kyr at Okataina and Taupo volcanic centres, Taupo Volcanic Zone, New Zealand. Journal of Volcanology and Geothermal Research, 148(3-4), pp.372-406.

590   Stokes, S., Lowe, D.J., Froggatt, P.C., 1992. Discriminant function analysis and correlation of late Quaternary rhyolitic tephra deposits from Taupo and Okataina volcanoes, New Zealand, using glass shard major element composition. Quaternary International, 13-14, pp.103-117.

Streck, M.J. and Wacaster, S., 2006. Plagioclase and pyroxene hosted melt inclusions in basaltic
595   andesites of the current eruption of Arenal volcano, Costa Rica. Journal of Volcanology and Geothermal Research, 157(1-3), pp.236-253.

Storm, S., Schmitt, A. K., Shane, P. and Lindsay, J. M., 2014. Zircon trace element chemistry at sub micrometer resolution for Tarawera volcano, New Zealand, and implications for rhyolite
600   1061 magma evolution. Contributions to Mineralogy and Petrology, 167(4):1000, DOI 10.1007/s00410-014-1000-z.

Sutton, A.N., Blake, S., Wilson, C.J. and Charlier, B.L., 2000. Late Quaternary evolution of a hyperactive rhyolite magmatic system: Taupo volcanic centre, New Zealand. Journal of the Geological
605   Society, 157(3), pp.537-552.

Tanaka, H.G.M.T., Turner, G.M., Houghton, B.F., Tachibana, T., Kono, M. and McWilliams, M.O., 1996. Palaeomagnetism and chronology of the central Taupo volcanic zone, New Zealand. Geophysical Journal International, 124(3), pp.919-934.

610

Tapia, C.A., Grant, G.R., Turner, G.M., Sefton, J.P., Naish, T.R., Dunbar, G. and Ohneiser, C., 2019. High-resolution magnetostratigraphy of mid-Pliocene (3.3–3.0 Ma) shallow-marine sediments, Whanganui Basin, New Zealand. Geophysical Journal International, 217(1), pp.41-57.

615 Tryon, C.A., Faith, J.T., Peppe, D.J., Fox, D.L., McNulty, K.P., Jenkins, K., Dunsworth, H. and Harcourt-Smith, W., 2010. The Pleistocene archaeology and environments of the Wasiriya beds, Rusinga Island, Kenya. Journal of Human Evolution, 59(6), pp.657-671.

Tryon, C.A., Logan, M.A.V., Mouralis, D., Kuhn, S., Slimak, L. and Balkan-Atlı, N., 2009. Building a
620 tephrostratigraphic framework for the Paleolithic of Central Anatolia, Turkey. Journal of Archaeological Science, 36(3), pp.637-652.

Turner, M.B., Bebbington, M.S., Cronin, S.J. and Stewart, R.B., 2009. Merging eruption datasets: building an integrated Holocene eruptive record for Mt Taranaki, New Zealand. Bulletin of
625 Volcanology, 71(8), pp.903-918.

Turner, M.B., Cronin, S.J., Bebbington, M.S., Smith, I.E. and Stewart, R.B., 2011. Integrating records of explosive and effusive activity from proximal and distal sequences: Mt. Taranaki, New Zealand. Quaternary International, 246(1-2), pp.364-373.

630

Turney, C.S., Blockley, S.P., Lowe, J.J., Wulf, S., Branch, N.P., Mastrolorenzo, G., Swindle, G., Nathan, R. and Pollard, A.M., 2008. Geochemical characterization of Quaternary tephras from the Campanian Province, Italy. Quaternary International, 178(1), pp.288-305.

635 Vandergoes, M.J., Hogg, A.G., Lowe, D.J., Newnham, R.M., Denton, G.H., Southon, J., Barrell, D.J., Wilson, C.J., McGlone, M.S., Allan, A.S. and Almond, P.C., 2013. A revised age for the Kawakawa/Oruanui tephra, a key marker for the Last Glacial Maximum in New Zealand. Quaternary Science Reviews, 74, pp.195-201.

640 Venables, W.N. and Ripley, B.D., 2002. Modern Applied Statistics With S., 4th edn.(Springer-Verlag: New York.).

Vu, V.Q., 2011. ggbiplot: A ggplot2 based biplot. R package version 0.55 http://github.com/vqv/ggbiplot

645

Vucetich, C.G. and Pullar, W.A., 1969. Stratigraphy and chronology of late Pleistocene volcanic ash beds in the central North Island, New Zealand. New Zealand Journal of Geology and Geophysics 12, pp.784-837.

650 Vucetich, C.G., Birrell, K.S. and Pullar, W.A., 1978. Ohinewai Tephra Formation; a c. 150000-year-old tephra marker in New Zealand. New Zealand Journal of Geology and Geophysics, 21(1), pp.71-73.

Walker, G.P.L. 1980. The Taupo plinian pumice: product of the most powerful known (ultraplinian) eruption? Journal of Volcanology and Geothermal Research, 8, pp.69-94.
655

Walker, G.P.L. 1981. Volcanological applications of pyroclastic studies. In Self, S., Sparks, R.S.J. (eds), "Tephra Studies". Reidel, Dordrecht, pp. 391-403.

Wallace, K. L., 2018, Alaska Tephra Data, 2018 (ver. 1.0, August 2018): U.S. Geological Survey data
660 release, https://doi.org/10.5066/P9PFQGVC (https://avo.alaska.edu/about/tephra.php)

Ward, W.T., 1967. Volcanic ash beds of the lower Waikato basin, North Island, New Zealand. New Zealand journal of geology and geophysics, 10(4), pp.1109-1135.

665 Watkins, N. D. and Huang, T. C., 1977. Tephras in abyssal sediments east of the North Island, New Zealand: chronology, paleowind velocity, and paleoexplosivity. New Zealand Journal of Geology and Geophysics, 20, pp.179-198.

Westgate, J.A. and Gorton, M.P., 1981. Correlation techniques in tephra studies. In Tephra studies (pp.
670 73-94). Springer, Dordrecht.

Westgate, J.A., Perkins, W.T., Fuge, R., Pearce, N.J.G. and Wintle, A.G., 1994. Trace-element analysis of volcanic glass shards by laser ablation inductively coupled plasma mass spectrometry: application to tephrochronological studies. Applied Geochemistry, 9(3), pp.323-335.
675

Westgate, J.A., Preece, S.J., Froese, D.G., Pearce, N.J., Roberts, R.G., Demuro, M., Hart, W.K. and Perkins, W., 2008. Changing ideas on the identity and stratigraphic significance of the Sheep Creek tephra beds in Alaska and the Yukon Territory, northwestern North America. Quaternary International, 178(1), pp.183-209.
680

Wickham, H., (2016). ggplot2: Elegant Graphics for Data Analysis. Springer-Verlag New York.

Wilson, C.J.N. and Rowland, J.V., 2016. The volcanic, magmatic and tectonic setting of the Taupo Volcanic Zone, New Zealand, reviewed from a geothermal perspective. Geothermics, 59, pp.168-187.
685

Wilson, C.J.N., Houghton, B.F., McWilliams, M.O., Lanphere, M.A., Weaver, S.D. and Briggs, R.M., 1995a. Volcanic and structural evolution of Taupo Volcanic Zone, New Zealand: a review. Journal of volcanology and geothermal research, 68(1-3), pp.1-28.

690 Wilson, C.J.N., Houghton, B.F., Pillans, B.J. and Weaver, S.D., 1995b. Taupo Volcanic Zone calc-alkaline tephras on the peralkaline Mayor Island volcano, New Zealand: identification and uses as marker horizons. Journal of Volcanology and Geothermal Research, 69(3-4), pp.303-311.

Wilson, C.J.N., Gravley, D.M., Leonard, G.S. and Rowland, J.V. 2009. Volcanism in the central Taupo
695 Volcanic Zone, New Zealand: tempo, styles and controls. In: Thordarson, T., Self, S., Larsen, G., Rowland, S.K., Hoskuldsson, A. (eds), 'Studies in volcanology: the legacy of George Walker'. Special Publications of IAVCEI (Geological Society, London), 2, pp.225-247.